SYMMETRICAL LASER CRYSTALS

SEMIANNUAL TECHNICAL SUMMARY REPORT

Period: 1 May 1964 - 1 December 1964

January 28, 1965

Contract Nonr-4131(00)
Program Code Number 3730
Authorization ARPA Order 306-62
Task Number NR017-708

SYMMETRICAL LASER CRYSTALS

SEMIANNUAL TECHNICAL SUMMARY REPORT

Period: 1 May 1964-31 December 1964

January 28, 1965

H. Kay - Group Leader
C. D. Brandle - Project Scientist
O. H. Nestor - Principal Investigator

This research is a part of Project DEFENDER under the joint sponsorship of the Advanced Research Projects Agency, the Office of Naval Research and the Department of Defense.

Union Carbide Corporation, Linde Division
Speedway Laboratories
P. O. Box 24184
Indianapolis, Indiana 46224

TABLE OF CONTENTS

LIST OF TABLES

LIST OF FIGURES

I. SUMMARY

Cubic perovskites should be desirable host crystals for "laser" dopant ions. A longer fluorescent lifetime is anticipated when the dopant is at a center of symmetry. Only four II-IV perovskite oxides have been proven to be cubic; they are $SrTiO_3$, $SrSnO_3$, $BaSnO_3$ and $BaZrO_3$. $BaZrO_3$ is predicted to be the best choice for doping with divalent rare-earth ions because the zirconium compound is more stable toward reduction. The synthesis of both $SrTiO_3$ and $BaZrO_3$ has been investigated in this program.

A self-containment or "skull-melting" method has been developed for fusing and maintaining melts of $SrTiO_3$ and $BaZrO_3$. The problems inherent in "skull-melting" have been studied both theoretically and experimentally. Stable melts of as much as 3 kg of both compounds have been made and controlled. Pulling experiments with $SrTiO_3$ have shown that the basic operations of the Czochralski method may be performed with skull-melts. Polycrystalline masses of $SrTiO_3$ have been "pulled" after nucleation on an iridium rod. The need for 'seed" material has prevented similar pulling of $BaZrO_3$. Seed rods have now been obtained and, with improvements in the starting procedure, it should be possible to pull pure and doped crystals of $BaZrO_3$.

II. INTRODUCTION:

The stated objective of this investigation is the growth of cm^3-sized crystals of cubic perovskites of type $A^{II}B^{IV}O_3$ activated with divalent or tetravalent dopant cations. Underlying this objective is the premise that the fluorescent lifetime of a dopant ion is greater when that ion is located at a center of symmetry in the crystal field than when it is asymmetrically located. This contract is recognized as a part of a greater effort under ARPA Order 306-62, Program Code Number 3730, 4730, to establish the validity of the premise and to determine to what extent fluorescent lifetimes can be effected.

Of the known perovskites, few appear attractive for this application. As discussed below and in the previous Annual Summary Report,[1] barium zirconate is thought to be potentially the best "host" for substitutional doping with divalent rare earth ions. This compound is extremely refractory and the usual techniques of making oxide crystals are not applicable. Previous experiments on flux growth of $BaZrO_3$ lead to the conclusion that a melt technique, or more particularly a Czochralski pulling method, would be more desirable, provided that a means of melting and containing this compound could be found. No crucible materials were known that could be used without attack at the required temperatures. The only way to contain a melt of $BaZrO_3$ appeared to be self-containment, in a "skull" of solid $BaZrO_3$. Initial experiments indicated that refractory oxides could indeed be kept molten in a skull of the same oxide, by direct coupling with a radio-frequency induction coil. These experiments also showed that there were many practical difficulties in skull-melting that had to be overcome before the method could be applied to crystal growth. A considerable portion of the present program has thus been devoted to development of the technology required in the skull-melting process. The remainder of this report describes in detail the chemical problems in the perovskites $SrTiO_3$ and $BaZrO_3$, the current state of development of the skull-melting technique and its application to Czochralski growth of pure and doped crystals of $SrTiO_3$ and $BaZrO_3$.

III. DISCUSSIONS OF PEROVSKITE SYSTEMS AS SYMMETRIC HOSTS FOR DOPANT IONS

A. "Cubic" Perovskites:

In order to fulfill the requirement that the dopant ion enter the lattice substitutionally in a site of high symmetry, the host perovskite should be cubic. A center of symmetry may exist in other crystal classes but, in the perovskites, a departure from cubic symmetry usually destroys this symmetry element. The perovskite structure is ideally the cubic structure obtained for a compound ABO_3 when the A atoms occupy the body center, the B atoms the corners and the O atoms the edge centers of the unit cube. (Alternatively, the unit cell may be centered on the B atom, with A atoms on the corners and the O atoms on the face centers of the cell). Despite the apparent simplicity of the perovskite structure, many ABO_3 compounds, including the mineral "Perovskite" ($CaTiO_3$) for which the structure is named, form crystals which are distortions of the ideal cubic structure. These distortions degrade the cubic symmetry to tetragonal, orthorhombic or rhombohedral symmetry and can be viewed as the result of slight displacements of the atoms from the cubic sites. Very frequently a single compound will undergo one or more first or second order polymorphic phase transitions when the temperature is decreased. The transitions are almost always to structures which are but slight distortions of the cubic structure. Many of these distorted phases are either ferroelectric or antiferroelectric. These interesting properties have stimulated research on perovskite systems, particularly the distorted structures, but are beyond the scope of the present study. It is convenient to refer to all such compounds, whether distorted or not, as "perovskites". As symmetrical hosts for dopant ions however, only those structures which are close to ideally cubic are of interest.

If an ideally cubic perovskite structure is to be formed, then the ions must obviously be of appropriate size. This leads to the concept of the "tolerance factor"* discussed in the previous report. This factor is very useful in making comparisons

*The tolerance factor "T" for a compound ABO_3, may be defined as;

$$T = \frac{1}{\sqrt{2}} \cdot \frac{(R_A + R_O)}{(R_B + R_O)}$$

where the R's are the ionic radii appropriate for the coordination numbers found in the perovskite structure.

between different compounds; the absolute value is, however, not a good measure of morphology. The ideal cubic perovskite should have a tolerance factor of exactly 1.00, but the values calculated from the customary lists of ionic radii are usually less than 1.00 for either cubic or distorted perovskites. The tolerance factor does not explicitly take account of the oxygen-oxygen distance, and pairs of appropriate values of R_A and R_B should satisfy the criterion equally well. Still another way of viewing the perovskite structure is that of a close-packed cubic array of oxygen ions with one fourth of these ions replaced by A ions. The B ions occupy one fourth of the octahedral voids. Thus, for an ideal perovskite, the **A** ion should be equal in size to oxygen or $R_A = R_O \simeq 1.40$ Å and the B ion should be of size given by $R_B = (\sqrt{2} - 1)\, R_O \simeq 0.58$ Å. In this ideal packing, the unit cell edge should be $2\sqrt{2}\, R_O$ or ca. 3.96 Å.

In order to see how real compounds obey these rules, examine the results obtained by Roth[2] who has made an extensive investigation of the structure of perovskites. In Table I below are listed all the $A^{+2}\, B^{+4}\, O_3$ perovskites that Roth determined to be cubic at room temperature. The table also gives the melting point, ionic radii,* unit cell edge and the tolerance factor calculated with and without regard to the coordination number of the A atom.

TABLE I

Cubic $A^{+2}\, B^{+4}\, O_3$ Perovskites

Compound	m. p. °C	R_A(Å)	R_B(Å)	a Å	T	T corr ⁄
$SrTiO_3$	2050	1.13	0.68	3.904	.86	.93
$SrSnO_3$	2100	1.13	0.71	4.034	.85	.92
$BaSnO_3$	ca2060	1.35	0.71	4.114	.92	1.00
$BaZrO_3$	2600	1.35	0.80	4.192	.88	.96

It is found that the geometric rules are only partially satisfied by these compounds. The corrected tolerance factor is close to unity, usually being slightly smaller. The unit cell is usually somewhat expanded and the R_B values are too large for

*Calculated ionic radii taken from (3). The radii are for 6-fold coordination and are very close to those used by Roth (2).

⁄ T_{corr} is the T value increased by 8% to correct for the 12-fold coordination of the A atom (1).

ideality. These departures from the rules are not unexpected and the agreement is probably as close as it should be for a simple "hard sphere" model of the ionic packing.

It is rather remarkable that of all the known perovskites only the four compounds listed in Table I have been shown to be cubic at room temperature. At higher temperatures several other compounds may transform to the cubic phase. For example, $BaTiO_3$ is cubic above its Curie point at ca 120°C. At lower temperatures even these compounds may undergo transitions to distorted phases. $SrTiO_3$ has been studied intensively[4, 5] and it has been shown to have a transition at 110°K to a very slightly distorted phase, and possibly two other transitions at lower temperatures. The low temperature properties of the other cubic compounds are in doubt.

Any of these cubic compounds should be satisfactory as a symmetrical host crystal from a geometrical point of view, provided that the dopant ions are of appropriate size to substitute into the lattice. The desired dopants are the divalent rare earths Sm^{+2}, Eu^{+2}, Yb^{+2} and possibly others, which should substitute into the A sub-lattice, and tetravalent ions such as Tb^{+4} or Mn^{+4}, which should substitute into the B-sublattice. The ionic radius of Eu^{+2} has been variously reported as 1.16 Å,[2] 0.03 Å less than Sr^{+2} or about 1.10 Å,[6] 1.16 to 1.21 Å[7] and 1.29 Å[3]. The radius of Sm^{+2} is expected to be slightly larger and that of Yb^{+2} and somewhat smaller than Eu^{+2} due to the "lanthanide contraction". These sizes are in between those of Sr^{+2} and Ba^{+2} and these ions should substitute into the A lattice of any of the cubic compounds without great difficulty. The radius of Tb^{+4} is given as 0.81 Å [3] while that of Mn^{+4} is 0.52 Å[3]. The Mn^{+4} radius is, therefore, somewhat small for the B position while Tb^{+4} is very nearly equal to Zr^{+4}. Finally, it is noted that none of the dopant ions given here are in the normal valence state for the element. The oxidation-reduction properties of the host and atmosphere must thus be considered when attempting to stabilize these dopant ions in the cubic perovskite host.

B. Crystal and Defect Chemistry of Cubic Perovskites:

Apparently there have been no comprehensive or definitive studies on the "defect" structure of cubic or pseudo-cubic perovskites. However, at least

one such study is now underway. R. E. Grace and L. C. Walters[8] at Purdue University have initiated experiments on the defect structure of $SrTiO_3$. Despite this lack of knowledge on the defect structure, there is quite a bit of empirical evidence on perovskites, particularly $BaTiO_3$ and $SrTiO_3$, that must be compatible with the defect structure and which can be used as a guide to anticipating the structure of these materials. Some of this evidence will be reviewed here, with particular regard to the compounds $SrTiO_3$ and $BaZrO_3$, because it appears that the usefulness of the cubic perovskites as hosts for the desired dopants may depend strongly on the defect structure of the host.

Several perovskites, including $SrTiO_3$, have been shown to exhibit anion deficiency or a departure from stoichiometry wherein the compound may be represented by:

$$A\,B\,O_{3-x} \qquad (1)$$

where: $x = o$ for ideal perovskite

$x \neq o$ for oxygen deficient structure.

In fact, Kestigian et al.[9] have shown that x may be as high as 0.5 for strontium titanate ($SrTiO_{2.5}$) prepared from strontium oxide and titanium sesquioxide (Ti_2O_3). It is very likely that this very wide range of oxygen deficiency is stabilized by the reduction of the titanium from Ti^{+4} to Ti^{+3}. Oxygen deficient strontium titanate may then be written as:

$$SrTi^{+4}_{1-2x}\ Ti^{+3}_{2x}O_{3-x} \qquad (2)$$

This view is supported by the fact that compounds such as $LaTiO_3$[9] and $CeTiO_3$[2] have been prepared, wherein the titanium is believed to exist in the trivalent state. Extensive studies by Buessem et al.[10, 11] have shown that the oxygen deficiency in rutile (TiO_2) is also explained by assuming reduction of Ti^{+4} to Ti^{+3}. Doping of $SrTiO_3$ with La^{+3} may be accounted for by a similar mechanism[9, 12] and the doped material is said to be an n-type semiconductor. Frederikse et al.[13] have investigated the transport properties of doped and "reduced" strontium titanate at low temperatures. Electronic or n-type conductivity is observed. It is noteworthy here that attempts to prepare reduced perovskites with zirconium in the B site, such as $LaZrO_3$, have been unsuccessful.[9] In the same study, attempts to produce lower oxides of

zirconium led to formation of the metal. It is, however, well known[14, 15] that oxygen ion vacancies occur in "stabilized" zirconias and that these are responsible for their ionic conduction. Finally, experiments on crystal growth at the Linde laboratories and elsewhere show that strontium titanate is oxygen-deficient when prepared by flame fusion but may be reoxidized to near stoichiometry by annealing in O_2 gas at a lower temperature.

These various facts and observations may be incorporated into a primative theory for the defects expected in the cubic perovskites. The following mechanisms have not been completely established and their validity remains to be proved. However, they appear reasonably in accord with presently available data and offer a guide to experimental work with cubic perovskites.

The basic perovskite lattice is co. idered to be largely (but probably not completely) ionic in binding. If the ionic crystal is in equilibrium with oxygen vacancies, and these in turn are in equilibrium with oxygen gas, the reaction may be written as follows, using "ionic" notation: (see reference 16)

$$A^{+2}\,B^{+4}(O^{-2})_3 \rightleftharpoons A^{+2}\,B^{+4}(O^{-2})_{3-x}\,(V_{O^{-2}}^{-2})_x + \frac{x}{2}\,O_2\,(g) \qquad K_3 \qquad (3)$$

The vacancies will tend to be strongly ionized according to:

$$(V_O^{-2}\text{-}2) \rightleftharpoons (V_O^{-}\text{-}2)^{\cdot} + e^- \qquad K_4 \qquad (4)$$

$$(V_O^{-}\text{-}2)^{\cdot} \rightleftharpoons (V_O\text{-}2)^{\cdot\cdot} + e^- \qquad K_5 \qquad (5)$$

If the B ions can exist in a reduced state then the reaction,

$$B^{+4} + e^- \rightleftharpoons (B^{+3})' \qquad K_6 \qquad (6)$$

can occur. Finally, the usual electronic equilibrium between electrons and holes may establish:

$$\text{Ground state} \rightleftharpoons \underset{(n)}{e^-} + \underset{(p)}{e^+} \qquad K_7 \qquad (7)$$

The condition for electroneutrality may be formulated as:

$$n + \left[(B^{+3})'\right] = p + \left[(V_{O^{-2}})^{\cdot}\right] + 2\left[(V_{O^{-2}})^{\cdot\cdot}\right] \qquad (8)$$

Since the compounds of interest are either good insulators or n-type semi-conductors, the value for p in equation (8) is probably small and may be eliminated, thus:

$$n + \left[(B^{+3})'\right] = \left[(V_{O^{-2}})^{\cdot}\right] + 2\left[(V_{O^{-2}})^{\cdot\cdot}\right] \qquad (9)$$

It is also quite possible that "complexes" of the B^{+3} ion and the vacancies may form, but these need not be treated explicitly here. Similarly other defects, such as B interstitials, may be possible but are neglected here.

The properties will depend strongly upon the equilibrium established in equation (6). It has been shown above that this reaction is probably very important for the titanates. A similar kind of reaction may be expected for the stannates, although here two electrons may be exchanged at once.

$$Sn^{+4} + 2e^{-} \rightleftharpoons (Sn^{+2})'' \qquad (10)$$

Such reductions have not been reported for the zirconates and in this respect $BaZrO_3$ should be more ideal than the other cubic perovskites.

The behavior toward dopant ions will also be strongly dependent on the defect structure. For example a trivalent impurity, I^{+3}, substituting into the A sub-lattice will act as;

$$(I^{+3}_{A^{+2}})^{\cdot} \qquad (11)$$

and should thus be added to the right side of equation (9), while substitution of a trivalent impurity into the B sub-lattice will produce;

$$(I^{+3}_{B^{+4}})' \qquad (12)$$

which will add to the left side of equation (9). The rare earths are all normally trivalent, but it is desired here to have the dopant substitute into the A sub-lattice without charge compensation. The rare earth must, therefore, be in the divalent state. Consider the equilibrium:

$$(Ln^{+3}_{A^{+2}})^{\cdot} + e^{-} \rightleftharpoons Ln^{+2}_{A^{+2}} \qquad K_{13} \qquad (13)$$

This reaction resembles equation (6) and the two reactions may be considered to be in competition, since both of the "oxidized" ions are competing for the electrons. Combining equations (6) and (13) one obtains:

$$\left[Ln^{+2}_{A^{+2}}\right]\left[B^{+4}\right] = \frac{K_{13}}{K_6}\left[(Ln^{+3}_{A^{+2}})^{\cdot}\right]\left[(B^{+3})'\right] \qquad (14)$$

In order to achieve the desired divalent doping, equation (14) requires that $K_{13}/K_6 \gg 1$. Recently, Schaufele and Weber[17] have reported on the "Vibronic Spectrum and Fluorescence Properties of Eu^{+3} in $SrTiO_3$". The fluorescence data clearly shows the europium to be trivalent, but there was no indication of the charge compensation mechanism. The compensating ion is probably Ti^{+3} as discussed above. In this example, it appears that the ratio K_{13}/K_6 is <u>not</u> large but probably less than unity. Since europium is one of the most easily reduced of the rare earths, it appears probable that equation (14) will always favor the products on the right when the B atom is titanium. Another way of stating this is to say that the divalent rare earths are better reducing agents (in the crystal) than is Ti^{+3}. It is expected that K_6 will be much smaller for $BaZrO_3$ and that the requirement for stabilization of the divalent state, $K_{13}/K_6 \gg 1$, can be met.

The dopants for the B sub-lattice are wanted in the tetravalent state. If lower states exist, there may be equilibria of the type:

$$(I^{+3}_{B^{+4}})' \rightleftharpoons I^{+4}_{B^{+4}} + e^{-} \qquad K_{15} \qquad (15)$$

The existence of lower oxidation states for B does not impede this reaction but may promote it. Thus the combination of equations (6) and (15) yields:

$$\left[I^{+4}_{B^{+4}}\right]\left[(B^{+3})'\right] = K_6 K_{15}\left[(I^{+3}_{B^{+4}})'\right]\left[B^{+4}\right] \qquad (16)$$

The condition for electroneutrality may be formulated as:

$$n + \left[(B^{+3})'\right] = p + \left[(V_{O}^{-2})^{\cdot}\right] + 2\left[(V_{O}^{-2})^{\cdot\cdot}\right] \qquad (8)$$

Since the compounds of interest are either good insulators or n-type semi-conductors, the value for p in equation (8) is probably small and may be eliminated, thus:

$$n + \left[(B^{+3})'\right] = \left[(V_{O}^{-2})^{\cdot}\right] + 2\left[(V_{O}^{-2})^{\cdot\cdot}\right] \qquad (9)$$

It is also quite possible that "complexes" of the B^{+3} ion and the vacancies may form, but these need not be treated explicitly here. Similarly other defects, such as B interstitials, may be possible but are neglected here.

The properties will depend strongly upon the equilibrium established in equation (6). It has been shown above that this reaction is probably very important for the titanates. A similar kind of reaction may be expected for the stannates, although here two electrons may be exchanged at once.

$$Sn^{+4} + 2e^{-} \rightleftharpoons (Sn^{+2})'' \qquad (10)$$

Such reductions have not been reported for the zirconates and in this respect $BaZrO_3$ should be more ideal than the other cubic perovskites.

The behavior toward dopant ions will also be strongly dependent on the defect structure. For example a trivalent impurity, I^{+3}, substituting into the A sub-lattice will act as;

$$(I_{A^{+2}}^{+3})^{\cdot} \qquad (11)$$

and should thus be added to the right side of equation (9), while substitution of a trivalent impurity into the B sub-lattice will produce;

$$(I_{B^{+4}}^{+3})' \qquad (12)$$

which will add to the left side of equation (9). The rare earths are all normally trivalent, but it is desired here to have the dopant substitute into the A sub-lattice without charge compensation. The rare earth must, therefore, be in the divalent state. Consider the equilibrium:

$$(Ln^{+3}_{A^{+2}})^{\cdot} + e^{-} \rightleftharpoons Ln^{+2}_{A^{+2}} \qquad K_{13} \qquad (13)$$

This reaction resembles equation (6) and the two reactions may be considered to be in competition, since both of the "oxidized" ions are competing for the electrons. Combining equations (6) and (13) one obtains:

$$\left[Ln^{+2}_{A^{+2}}\right]\left[B^{+4}\right] = \frac{K_{13}}{K_6}\left[(Ln^{+3}_{A^{+2}})^{\cdot}\right]\left[(B^{+3})'\right] \qquad (14)$$

In order to achieve the desired divalent doping, equation (14) requires that $K_{13}/K_6 \gg 1$. Recently, Schaufele and Weber[17] have reported on the "Vibronic Spectrum and Fluorescence Properties of Eu^{+3} in $SrTiO_3$". The fluorescence data clearly shows the europium to be trivalent, but there was no indication of the charge compensation mechanism. The compensating ion is probably Ti^{+3} as discussed above. In this example, it appears that the ratio K_{13}/K_6 is not large but probably less than unity. Since europium is one of the most easily reduced of the rare earths, it appears probable that equation (14) will always favor the products on the right when the B atom is titanium. Another way of stating this is to say that the divalent rare earths are better reducing agents (in the crystal) than is Ti^{+3}. It is expected that K_6 will be much smaller for $BaZrO_3$ and that the requirement for stabilization of the divalent state, $K_{13}/K_6 \gg 1$, can be met.

The dopants for the B sub-lattice are wanted in the tetravalent state. If lower states exist, there may be equilibria of the type:

$$(I^{+3}_{B^{+4}})' \rightleftharpoons I^{+4}_{B^{+4}} + e^{-} \qquad K_{15} \qquad (15)$$

The existence of lower oxidation states for B does not impede this reaction but may promote it. Thus the combination of equations (6) and (15) yields:

$$\left[I^{+4}_{B^{+4}}\right]\left[(B^{+3})'\right] = K_6 K_{15}\left[(I^{+3}_{B^{+4}})'\right]\left[B^{+4}\right] \qquad (16)$$

Reactions of this type may put the dopant in the desired valence state but only by creating other imperfections $(B^{+3})'$ in the neighborhood. The best situation will be when both ions are in their oxidized state. This requires removing electrons and decreasing the oxygen vacancies by increasing the partial pressure of oxygen gas. In attempting to dope into the B sub-lattice, with Mn^{+4} for example, the main problem is whether or not the desired partial pressure of oxygen can be obtained in the experiment. If this partial pressure is one atmosphere or less there should be no difficulty, but partial pressures in excess of one atmosphere would necessitate the use of special "high pressure" apparatus.

C. Growth Methods:

Of the four cubic perovskites, $SrTiO_3$ and $BaZrO_3$ were chosen for intensive study. Initial experiments indicated that the stannates would be just as difficult to prepare and would be subject to the same problems of crystal chemistry as the titanates, as described above. $BaZrO_3$ was thought to offer the best potential as a host material, but it was apparent that it would be quite difficult to make due to its very high melting point. The fusion of $SrTiO_3$ is more easily accomplished, and study of the melt growth of this compound was continued as a pilot substance for the studies with $BaZrO_3$, despite the fact that other modes of synthesis, such as flame fusion, are applicable. Furthermore, this compound is still of interest as a host for tetravalent dopants as described above.

The most recent phase diagrams published in "Phase Diagram for Ceramists"[18] for the binary oxide systems $SrO-TiO_2$ and $MO-ZrO_2$ (including $BaO - ZrO_2$) are shown in Figure 1. These diagrams show that both $SrTiO_3$ and $BaZrO_3$ have congruent melting points and may, therefore, be prepared from melts of stoichiometric composition. Measurements made in the Linde laboratories indicate that the melting point of $SrTiO_3$ is ca 2050°C or close to that shown in the upper diagram in Figure 1. The right hand diagram in Figure 1 indicates that the melting point of $BaZrO_3$ exceeds 2600°C. No precise measurements of the exact melting point have been made but we have measured a liquidus temperature of ca 2600°C for a near-stoichiometric melt. This agrees well with Figure 1. This literature data is quite old but still seems to be the best available. There is no indication of what "fine structure" may be present in

the phase diagram, or whether or not compounds are formed in addition to the 1:1 compound.

The possible methods for growing these compounds are not numerous. Flame fusion or the Verneuil technique, Czochralski "pulling" and growth from fluxes have all been considered. Strontium titanate can be grown by flame fusion, but flame temperatures high enough to melt $BaZrO_3$ are not available. Flux methods do not usually produce as sizeable crystals as the other techniques, and flux inclusion is frequently a serious problem. The results of experiments with all three methods have been described in the previous Annual Summary Report[1]. It was concluded therein that the Czochralski method offered the most promise. However, these compounds are difficult to contain when molten, and there appear to be no truly inert crucible materials to use. Strontium titanate has been fused in iridium crucibles in the Linde laboratories and elsewhere[19]. Our results were not completely satisfactory; there was always some evidence of reaction with the crucible and contamination of the melt. Barium zirconate cannot, of course, be melted in iridium. Two additional techniques appear to be available for melting these refractory and oxidizing materials. One involves operating appreciably off stoichiometry in the $AO-BO_2$ system (see Figure 1) and thus depressing the melting point sufficiently so that more traditional crucible materials may be employed. Barium titanate, strontium titanate and a variety of other perovskites have been pulled from platinum in this manner[20]. For strontium titanate the composition must be set fairly close to the lower eutectic in order to stay below the melting point of platinum. It is conceivable that the same type of thing could be done with $BaZrO_3$ by adding a large excess of either ZrO_2 or BaO and containing the melt in iridium (or even platinum if the diagram of Figure 1 is valid). The phase diagram is so poorly defined that these predictions are very uncertain. The other possibility is that of containing the melt in a solid shell or "skull" of its own composition "Skull melting" has sometimes been applied to metal and semi-metal fusions and offers the obvious advantage that contamination from crucible materials is avoided. In order to apply this technique to refractory oxide systems, it is necessary to find means for supplying the thermal energy required for melting and holding the charge. When a

crucible is used, it may be externally heated, or it may be used as a radio-frequency susceptor to supply the requisite heat. In the skull-melting process all the heat cannot be supplied from the outside. Conversely, if inert crucible materials are not available, then there are no inert materials for use as internal susceptors. The solution to this problem appears to be to use the molten liquid as its own susceptor and couple it directly to a radio-frequency, induction-heating power source. Van Arkel et al.[21] have shown that the electrical conductivities of molten oxides are of the same order as that of the molten halides. It should therefore be sufficient to allow coupling of the energy from an r-f generator. The feasibility of direct coupling to oxide melts was demonstrated by Monteforte et al.[22] who maintained melts of manganese ferrite in an r-f coil. Initial experiments conducted at Linde were encouraging; it was found that very refractory substances could be fused. The potential advantages of the skull-melting technique, (a) absence of crucible and other possible contaminants, (b) applicability to extremely refractory materials, and (c) ability to operate in different "atmospheres" including strongly oxidizing atmospheres, appeared very attractive. The application of this technique to the melting of $SrTiO_3$ and $BaZrO_3$ is discussed in detail in the next section.

IV. DEVELOPMENT OF "SKULL-MELTING" TECHNIQUE FOR CZOCHRALSKI CRYSTAL GROWTH

A. General Concept of Skull-Melting as Applied to Refractory Oxides:

The compounds of interest are insulators or semiconductors at low temperatures. Thus the interaction of these solids with an electromagnetic field will differ from that of metals or other conductors. No currents, other than displacement currents, will circulate in these materials and there will be little if any Joule heating of these substances. Such solids are not heated appreciably by placing them in a radio-frequency induction coil. In one respect this is advantageous. The skull-melting concept requires that the molten material be surrounded by the solid oxide. In induction heating, as well as many other methods of heating, most of the power tends to be dissipated in the outer layers of the object. If the solid skull conducted electricity, it would be impossible to establish a stable skull by coupling to an external coil. On the other hand, the molten oxides must have an appreciable electrical conductivity so that the necessary power may be dissipated. This condition can usually be satisfied, if a high-frequency power source is used. It is therefore valid to consider the liquid oxide as a conductor of conductivity σ, while treating the solid as an insulator ($\sigma_{solid} = o$). In order to quantitatively determine the power delivered to the melt, it is in general necessary to solve Maxwell's equations for the particular geometry. If a cylindrical symmetrical geometry is employed, solutions may be obtained in the form of complex Bessel functions (see section B below). There are aspects to skull-melting that limit the usefulness of this general approach. The geometry is usually not truly symmetrical, showing at least asymmetry from top to bottom. The values of the electrical conductivity, σ, of oxide melts are usually only approximately known, if at all, and it may be a strong function of composition and temperature. Most important, however, is the fact that the interface between the melt and the solid skull is not prescribed but is variable and dependent on a balance in the energy flows. Approximate "engineering" solutions appear to be more useful than the direct application of Maxwell's equations. This problem is treated in section B.

The stability of the skull depends on the establishment of a steady state energy balance. At least part of the input energy will be dissipated in the thermal flux flowing out through the skull. This energy flow decreases the efficiency of the process but must occur in the steady state. It is not apparent, a priori, that all skull geometries can be stable. This question is treated in section D, wherein it is shown that stability depends on the relative skull thickness and on the electrical conductivity of the melt. If the thickness becomes too large or the conductivity too low the skull boundary becomes unstable.

The formation of the skull presents problems. The desired material is usually not readily available as a dense material preformed to the proper size and shape. Frequently, one is forced to start with a powder. While in certain cases it might be desirable to make special sintered ceramic shapes, the problem of stabilizing the skull cannot be avoided. The experiments described here have been conducted with fine powders as the starting material, the formation of the skull occurring in situ. It has been found by experiment, however, that it is desirable to have some form of auxiliary "container" to confine the charge and prevent the fluid melt from running out during formation of the skull. Inert dielectric materials, that can withstand the conditions, are not available. These auxiliary parts have therefore been built of copper and are water-cooled to prevent them from melting. The auxiliary container cannot, however, function as a susceptor or electrical short-circuit, because the coupling of power to the melt would then be lost. The two requirements of confinement, and not short-circuiting the power, are in conflict. A satisfactory solution must therefore be a compromise, and the auxiliary container design is complicated. Many designs have been conceived and empirically tested. Satisfactory compromises have been achieved and the important features of their design established.

Since the entire purpose of the skull-melting technique is to obtain oxide melts from which crystals can be pulled, the problem of controlling the melt size and temperature must be solved. This must be done by controlling the electrical power delivered to the melt. The skull-melting process has a degree of freedom less than more conventional melting processes, since the solid-liquid interface is a phase

boundary. For crystal synthesis a phase boundary must also exist at the interface of the growing crystal. In high temperature systems, the crystal interface frequently is the lowest temperature in the melt, a temperature gradient being established to the wall. It is not apparent how this can be compatible with a second phase boundary at the skull. The answer has been found by experiment. It can be demonstrated that it is possible to maintain temperature gradients in a melt such that the interface at a crystal being pulled and the skull are both in dynamical equilibrium. The range of control may, however, be somewhat limited by the second phase boundary.

B. Electrical Coupling to Melts:

If the experimental geometry can be reasonably approximated by a semi-infinite cylindrical geometry, then the Maxwell field equations (23) reduce to:

$$\frac{\partial E_\theta}{\partial r} + \frac{E_\theta}{r} = -\frac{\partial B_z}{\partial t} \qquad (17)$$

$$J_\theta = -\frac{\partial H_z}{\partial r} - \frac{\partial D_\theta}{\partial t}$$

By making the substitutions $D = \epsilon E$, $B = \mu H$ and $E = J/\sigma$, these equations reduce to relations between the current density and magnetic field:

$$\frac{\partial}{\partial r}\left(\frac{J_\theta}{\sigma}\right) + \frac{J_\theta}{r\sigma} = -\mu\left(\frac{\partial H_z}{\partial t}\right) \qquad (18)$$

$$J_\theta = -\left(\frac{\partial H_z}{\partial r}\right) - \epsilon \frac{\partial}{\partial t}\left(\frac{J_\theta}{\sigma}\right)$$

In the general case the electrical conductivity, σ, may be a function of temperature and, hence of r, if there are thermal gradients. Furthermore if the conductivity is very low, the relaxation time ϵ/σ may be large in relation to the frequency leading

to "displacement currents". This would be the case for a good dielectric. For any appreciable conductivity, however, the last term in the lower equation (18) vanishes and, to the extent that the conductivity may be considered constant, the equations combine to:

$$\left(\frac{\partial^2 H_z}{\partial r^2}\right) + \frac{1}{r}\left(\frac{\partial H_z}{\partial r}\right) - \mu\sigma\left(\frac{\partial H_z}{\partial t}\right) \qquad (19)$$

For sinusoidal fields, $\partial H_z/\partial t = jwH_z$, and this equation (in rationalized m.k.s. system) is equivalent to that given by Simpson [24]. Simpson shows how equation (19) may be solved in terms of the complex Bessel functions; ber, bei, ber', bei'. The result for the field, H_z, inside the "workpiece", relative to that at the surface, H_{zo} where r = a, is given by:

$$\frac{H_z}{H_{zo}} = \frac{\text{ber } kr + j \text{ bei } kr}{\text{ber } ka + j \text{ bei } ka} \qquad (20)$$

where $k = (\omega\mu\sigma)^{1/2}$

The relative current density is found from equations (20) and (18) and is:

$$\frac{(J_\theta)_r}{(J_\theta)_a} = \frac{\text{ber' } kr + j \text{ bei' } kr}{\text{ber' } ka + j \text{ bei' } ka} \qquad (21)$$

These results may now be developed for various cases to determine the total flux and power in cylindrical "workpieces". Many examples of this type of calculation are given by Simpson (24). The concept of the "skin-depth" or "penetration depth" is frequently used in these high-frequency calculations. The skin depth, δ, may be defined by,

$$\delta = \left(\frac{2}{\omega\mu\sigma}\right)^{1/2} \text{ , meters,} \qquad (22)$$

and represents the effective average depth of penetration of the current. For relatively small values of δ, the actual current distribution may be approximated by a uniform current throughout the depth δ. Similarly, the effective r - f resistance of an actual circuit may be calculated from an analogous circuit whose depth is δ using d - c values for the resistivity. For sufficiently large values of $\omega\mu\sigma$, and thus for a small

skin depth, the Joule heating may be reasonably assumed to occur in the "skin". When the depth is large, relative to the radius of the cylinder, the current distribution must be evaluated. For a melt, however, stirring by convection occurs and knowledge of the total power delivered is more important than knowing the spatial distribution.

Equations (20) and (21) may be evaluated from tabulated values of ber, bei and their derivatives (24, 25) but these expressions are rather inconvenient to use when the properties and dimensions of the object are variable. What is really desired is to know how to couple a melt to an induction coil in the tank circuit of a radio-frequency power oscillator. The coil, and the conductive objects inside it, may be considered as a complex inductance wherein the "loss" term is responsible for the power dissipation or Joule heating. However, the calculation of the complex inductance also requires evaluating Bessel functions. Fortunately, a very similar problem is encountered in "eddy current" testing of materials. (26) Conductive objects, usually cylindrical, are placed inside an induction coil and the impedence change in the circuit is measured. It is desired to observe and identify variations in size and conductivity and to detect flaws or voids in the object. The development and application of this method of testing is described at length in reference[25], following the extensive work of Förster[27]. Förster has evaluated the functions and shown how the behavior of a coil and load may be conveniently expressed in terms of a "complex effective permeability", which will depend on the permeability, conductivity and dimensions of the object and on the frequency. The latter quantities may be combined to a single variable, F. A plot of the real and imaginary parts of the complex effective permeability as a function of F, is shown in Figure 2. The complex effective permeability is the permeability of a fictitious substance that would behave as the actual load. There are several interesting aspects to Figure 2. At very low values of σ and f the coil is uneffected; $K_m' = 1$ and $K_m'' = 0$ as for free space. At higher values of F, K_m' decreases, K_m'' increases and a maximum loss occurs at F = ca. 6. At high values of F both K_m' and K_m'' decrease. Furthermore, it may be noted that the quality factor for the coil, $Q = \omega L/R = K_m'/K_m''$, is never less than unity (for a homogeneous cylinder; the problem differs for tubing), although the reactance and resistance will both vanish together for large F. In Figure 2, the loading object is treated as completely filling the coil; this is usually not so in practice. The cylindrical load, or

"workpiece", is often considerably smaller than the coil. The filling factor, η , or the cross section of the work relative to the coil must be considered. When the filling factor is less than unity the curve of Figure 2 shrinks uniformly toward the point $K_m' = 1$ on the ordinate. The resultant curves are given in references [26] and [27], (see also Figure 3). It is now convenient to relocate the origin at $K_m' = 1$, $K_m'' = 0$, and plot a "complex plane map" in terms of $\eta (1-K_m')$ and $\eta K_m''$. Such a map is shown in Figure 3. The variables in this graph are η , F and σ , which for non-magnetic loads are defined by:

σ = electrical conductivity of object (mho/m) (23)

$$\eta = \text{filling factor} = \left(\frac{d}{D}\right)^2 \quad (24)$$

where: d = object diameter, m
and D = coil diameter, m

$$F = \frac{\sigma d^2 f}{5.066 \times 10^5} = \frac{\sigma \eta D^2 f}{5.066 \times 10^5} \quad (25)$$

where: f = frequency in c.p.s

The quantities η and F are dimensionless parameters. In Figure 3, the spade-shaped curves are lines of constant η ; the radial lines are lines of constant F and the remaining curves are drawn for constant ratio of F/η . If the diameter of the coil and the frequency are fixed, these latter lines represent lines of constant conductivity, σ .

Finally, it may be shown that the ordinates in Figure 3 are related to the effective electrical properties of the coil by the relations:

$$\eta (1 - K_m') = 1 - \frac{\omega L}{(\omega L)_o} \quad (26)$$

$$\eta K_m'' = \frac{R}{(\omega L)_o}$$

where: $(\omega L)_o$ = coil reactance without load, ohms

ωL = coil reactance with load, ohms

R = effective series resistance of coil with load, ohms

The curves and equations used in eddy current testing were originally developed for treating long cylindrical bars placed coaxially inside a solenoidal induction coil. These same relations will be used here, without alteration, to approximate inductive coupling to melts, although the geometry may not be as ideal. The effects of melt diameter, melt conductivity and frequency are shown directly by Figure 3. In practice it is difficult to make the filling factor, η , large and therefore only half of the complete diagram is given. Furthermore, radio-frequency oscillators operate at rather low power factors ($Q \gg 1$) and there is no advantage in striving for extremely tight coupling. Joule heating will only result from the resistive or loss part of the impedance, corresponding to the abcissa in Figure 3. It is seen that there is a maximum loss allowable for each value of η , corresponding to F = ca. 6. This does not, however, correspond to constant conductivity. The conductivity required for maximum loss will vary with η . In most induction heating applications involving metals, the conductivity is much larger than this maximum loss value. The load is then largely inductive, and lies close to the ordinate in Figure 3. Although the loss may be relatively small, heating is accomplished by the very large circulating current in the tank circuit of the oscillator. In this part of the diagram, variations in σ and η produce different effects. The behavior of poor conductors is quite different. Such loads lie near the bottom of the diagram. The inductive reactance is only slightly effected and increases in σ and η both tend to increase the loss in about the same way. If the melt has a constant diameter, but is allowed to increase in conductivity, it is possible to have the loss increase to a maximum (at $F \simeq 6$) and then decrease again. This type of reversal can result in instability. There is evidence that such behavior can occur in certain skull-melting experiments. It is thought to be advantageous to operate above the maximum loss region in the diagram, or in other words one wants $F > 6$. The conductivity, σ, is not usually alterable and η is made as large as practical. The size (as given by D) or the frequency, f, must be increased to increase F. For a given frequency, there will be a minimum size for the melt and conversely, experiments on small charges will require high frequencies. The dissipation of thermal energy will also depend on the scale of the experiment and an energy balance must be made to determine the power requirements.

C. Electrical Conductivities of Melts:

There have been very few measurements made to determine the conductivity of molten oxides. Van Arkel et al.[21] review the subject and report measurements on eight oxides (LiO, Bi_2O_3, TeO_2, PbO, MoO_3, V_2O_5, CrO_3 and Sb_2O_3). Some additional "electric furnace" estimates are given for refractory oxides (MgO, CaO, TiO_2, ZrO_2, ThO_2, Cr_2O_3 and Al_2O_3). The conductivities vary with temperature approximately according to an equation of the usual type;

$$\log \sigma = A + \frac{B}{T} \tag{28}$$

from which activation energies may be calculated. Some of Van Arkel's results are shown in Figure 4 along with other data on various metals, semi-conductors, salts, aqueous solutions etc. for purposes of comparison. Some data on solid CaO, ZrO_2 and $CaZrO_3$ from Johansen and Cleary[14] are also shown. Although the high temperature data may be inaccurate, it appears that the molten oxides of interest should have conductivities of the order of 10^3 to 10^4 mho m^{-1}. They should then be better conductors than molten NaCl and the strongest of aqueous solutions, but poorer conductors than carbon and the metals. Figure 4 also shows that salt 'NaCl) is a fairly good insulator when solid and the change in conductivity on fusion is about 4 orders of magnitude. A lesser change is shown for MoO_3. The data on "stabilized zirconias"[14] indicates that CaO, ZrO_2 and $CaZrO_3$ acquire appreciable conductivity before melting and the change on fusion may not be great. This is important, since skull-melting depends on having a dielectric solid skull. Nevertheless, experiments have proved that the extent of the solid conductivity in $SrTiO_3$ and $BaZrO_3$ is not sufficient to destroy the skull-melting process.

The conductivity data may be used to estimate the frequency required. Equation (25) may be rearranged to (approximately):

$$2f\,(mc) = \left(\frac{F}{\eta}\right)\left(\frac{1}{\sigma D^2}\right) \tag{29}$$

Calculating for a 5-inch diameter, $\sigma = 10^3$ mho/m and a filling factor of 0.6, the frequency required for F = 6 is found to be about 310 kc. This is fortunately a convenient frequency for induction heating equipment. However, reducing the size or filling factor will necessitate higher frequencies. Our experiments have been conducted at two frequency regions ca. 350 Kc. and ca. 3 Mc. Satisfactory coupling to $SrTiO_3$ and $BaZrO_3$ was obtained at both frequencies but the higher frequency is preferred because it permits smaller scale experiments.

D. Criteria for Stability:

Joule heating will occur in the melt due to the electrical power dissipated there. This power is given by:

$$P_E = I^2R = I^2 (wL)_o (\eta K_m'') \equiv I^2 (wL)_o p_E \qquad (30)$$

The function, $p_E = (\eta K_m'')$, may be obtained from Figure 3 if the conductivity is known. The function will depend on the filling factor, η, and therefore on the radius of the melt relative to that of the coil. The dependence of p_E on η or on $r = r_m/r_o$ is shown in Figure 5 for various fixed values of the ratio F/η, corresponding to constant conductivity. It is seen that the value of p_E drops rather quickly with decreasing radius or , but that the rate of decrease is less for larger values of F/η.

The total electrical power, P_E, delivered to the melt will ultimately be dissipated by heat or other forms of energy flowing out of the system. In high temperature melts, an appreciable amount of this energy loss is by radiation from the surface of the melt. Another portion of the input power will be dissipated by thermal conduction through the wall of the skull. Since the melt-solid interface is not fixed and since both the input power and heat losses increase with increasing melt diameter, it is necessary to inquire whether or not the interface is stable, and if so, what conditions are required for stability.

The radiation loss or power, P_R, may be written as:

$$P_R = e\alpha T_m^4 \pi r_m^2 \equiv e \alpha T_m^4 \pi (p_R) \qquad (31)$$

where:
- e = emissivity of melt surface
- α = Stefan - Boltzmann constant = 5.685×10^{-8}, watt/$m^2 {}^oK^4$
- T_m = melt temperature, ^oK
- r_m = melt radius , m
- $p_R \equiv r_m^2$

It is assumed that the melt temperature is uniform, due to mixing of the melt, and equal to the melting point. No recovery of the radiation is considered.

If the skull has a uniform thermal conductivity, k, and the outside of the skull is in contact with a "cold wall" maintained at a fixed low temperature, T_o, then the power loss by thermal conduction, P_T, may be expressed as:

$$P_T = \frac{2\pi z k (T_m - T_o)}{\ln (r_o / r_m)} \equiv 2\pi zk (T_m - T_o) (p_T) \qquad (32)$$

where:
- k = thermal conductivity, watts/m ^oK
- z = length , m
- r_o = outer radius of skull
- r_m = melt radius
- T_o = "cold wall" temperature
- $p_T = \frac{i}{\ln \frac{r_o}{r_m}}$

It is noteworth that, unlike equation (31), equation (32) depends only on the relative skull thickness and not on the absolute size. Thus, none of this power can be saved by scaling down (in radius) and, conversely, no more will be required in scaling up (in radius). Considering only these processes, an approximate energy balance can

be written by equating input and output powers. In the steady state:

$$P_E = P_R + P_T \tag{33}$$

Furthermore, stability of the melt radius, r_m, requires:

$$\frac{dP_E}{dr_m} < \frac{dP_R}{dr_m} + \frac{dP_T}{dr_m} \tag{34}$$

These two equations may be combined, in terms of the functions, p_E, p_R, p_T and the radius ratio, $r = r_m/r_o$, to yield:

$$\frac{1}{p_E}\left(\frac{dp_E}{dr}\right) < \frac{\frac{1}{p_R}\left(\frac{dp_R}{dr}\right)}{1 + \frac{P_T}{P_R}} + \frac{\frac{1}{p_T}\left(\frac{dp_T}{dr}\right)}{1 + \frac{P_R}{P_T}} \tag{35}$$

which becomes:

$$\frac{1}{p_E}\left(\frac{dp_E}{dr}\right) < \frac{1}{r}\left[\frac{2}{1 + \frac{P_T}{P_R}} + \frac{p_T}{1 + \frac{P_R}{P_T}}\right] \tag{36}$$

The left hand quantity is evaluated graphically, in terms of the parameter F/η (constant σ); some representative curves are plotted in Figure 6. In all cases, the value decreases with melt radius. If radiation is the major source of dissipation, the first term on the right dominates and becomes simply $2/r$. This, of course, also decreases monotonically as shown in Figure 7. If conduction is the major dissipative process, then the second term dominates and becomes p_T/r. This function has been evaluated and is plotted in Figure 8. This function approaches infinity at both $r = 0$ and $r = 1$, and shows a broad minimum at $r =$ ca. 0.4. When both radiation and conduction are

important the effect of each must be adjusted as given in equation (36). Comparison of Figures 6, 7 and 8 shows that small values of the melt radius ratio r, are unstable. If radiation controls, it also appears that the value of F/η must be about 10 (in order to have the curves of Figure 6 below that in Figure 7). When conduction controls, relative radii greater than ca. 0.5 appear to be stable for high-conductivity melts, larger values being required for poorer conductivities. It is concluded that the melt radius, r_m, must not be too small; thick skulls can be unstable. The best results are anticipated with relatively thin skulls and high values of F/η .

The magnitude of the power required for skull melting may be estimated from equations (30-33). For example, application of equation (31) to $BaZrO_3$ at 2600°C, with a melt radius of 3 cm, and assuming unit emissivity, results in a power of 11 Kw. The dissipation by thermal conduction is more difficult to estimate. Again using $BaZrO_3$ as an example and applying equation (32) for z = 0.1 m, T_m = 2600°C, T_o = 100°C, and r = 0.7, one obtains $P_T \simeq 4 \times k$ kilowatts. The value will depend on the effective thermal conductivity, k, in watts per meter per degree. If "crystal" values are taken for the thermal conductivity, very high powers result. However, the skull material will not usually be in large crystals but may be of very fine grain structure and highly disordered. Such a skull will have a much lower effective k than the crystalline material. Nevertheless, this may be a problem with certain materials that tend to form a crystalline wall. If possible, one would like to keep the effective conductivity, k, of the order of unity (watts/m °K). Experiments with perovskites indicate that this is not a major problem, but it appears that other substances may be different.

In summary, not all skulls are stable but the range of stability is sufficient provided that r is not too small and F/η is high enough. The total power required may be substantial, perhaps 20 kw or more, due to high losses by radiation and thermal conduction. A rather large rf power source may be needed. In this work, a Lepel generator capable of delivering 50 Kw was employed. This generator is a Class-C oscillator with a 6696 triode. The work coil is part of the "tank" coil in the oscillator. Several frequency ranges (200-450 Kc, 2-5 Mc, and 5-8 Mc) are available. Frequencies of 350 Kc

and ca. 3 Mc have been most often used. It is estimated that powers exceeding 20 Kw have been delivered in certain of the skull-melting experiments.

E. Control of Melts for Crystal Pulling

As in all forms of melt-pulling, the conditions must be well controlled if high quality single crystals are to be made. In the more common systems everything, except the melt level and the pulled crystal, remains fixed in position. The temperature at various locations may be monitored and used for control purposes. A common procedure is to measure the crucible temperature with an optical pyrometer, and use that signal for controlling the generator. This procedure is, of course, not possible in skull-melting where there is no crucible. The only place where a temperature can be taken is the top surface of the melt. Manual measurement of the surface temperature of the melts has been made in almost all the experiments, but so far it has not proven feasible to use the melt surface temperature in automatic control. A considerable effort has been devoted to measuring and controlling the electrical output of the generator. The present instrumentation includes:

a) Meters to indicate the d-c plate voltage, E_b, plate current, I_b, grid current, I_c, and rms r-f output current, I. This instrumentation was supplied with the Lepel generator. A magnetic amplifier and saturable core reactor was also included. The reactor control current is also monitored.

b) A Jennings capacitive voltage divider to reduce the coil voltage, e, for measurement on a Tektronix 551 Cathode Ray Oscilloscope; pick up coils for similarly displaying the r-f current, i, on the other channel; a G-R, r-f signal generator for monitoring the frequency. The peak values, modulation index and approximate rms values may all be obtained from the oscilloscopic traces.

c) A control console which includes rectifiers and filters to "detect" both the r-f current (from a pick up coil) and the r-f voltage (from the CRO) and attenuate these signals for display on millivolt indicators or recorders; a d-c servomultiplier constructed from an L and N model H indicator; two Honeywell recorder controllers; Honeywell set-point and deviation amplifier and current controlling rate-proportional-reset controller. This console permits recording and controlling from any of the measured signals. Furthermore a "product" signal may be generated from two of the measured quantities and used for control. The "ratio" may also be recorded. Provision has also been made for recording the controller output.

d) A shunt in the d-c plate circuit provides a "plate current" signal for control purposes.

e) Input circuits to the control console to permit any other d-c signal, such as that from an optical pyrometer, to be used for control.

The reason for this rather extensive instrumentation is that it was not obvious, a priori, which of several signals would be best to control. The present set-up is extremely versitile, and permits using almost any of the measured variables for control purposes.

Many attempts have been made to measure and control the "output power" of the generator. This power is $I^2 R$, where R is the effective resistance given in equation (27) and corresponds to the horizontal displacement in Figure 3. If the inductive reactance did not also change, the task would be simple. In fact various approximate methods for measuring the "real" component of the impedance have been tested and used, including comparison of e and i in a "phase-sensitive detector circuit" (part of the rectifier section of the control console). The accuracy of this, and all other simple methods, is degraded by the change in frequency of the oscillator as the load changes. Were this frequency constant, accurate output power measurement could be made. As it is, only a crude

approximation can be obtained.

Two methods of control have been found most useful in skull-melting. They are control of r-f output current (or alternatively the current-voltage product) and control of the d-c plate current. Since all power comes from the current circulating in the primary coil all coupling may be related to this r-f current. However, the plate current is a more sensitive measure of the loading of the oscillator. All these methods have been used and will be used in future crystal growing experiments. The best control method will be selected empirically as the one capable of producing the best crystals.

It has been demonstrated repeatedly that the generator can be controlled so as to hold a melt of $SrTiO_3$ in an apparent steady state. Furthermore, a solid "island" may be maintained in the center of a melt at the cooler central region. Crystalline solid can be "pulled" from this central region. It is concluded that the skull <u>is</u> compatible with thermal gradients necessary for crystal growing. An analysis of the complex situation prevailing when both the skull and crystal must be in "phase-equilibrium" has been deferred in favor of empirical testing of the melting and pulling processes.

V. EXPERIMENTAL RESULTS AND MATERIALS

A. Skull-Melting of $SrTiO_3$ and $BaZrO_3$

Many of the experimental results have already been mentioned in the previous discussions. A summary of the tests on $SrTiO_3$ and $BaZrO_3$ is shown in Table A. The experiments are reported in chronological order. Many exploratory tests have been omitted, as have several experiments which were made on other substances to obtain information to guide the work on the perovskites. Unfortunately, the actual melting runs, in work of this nature, only account for a fraction of the experimental time. Until repetitive procedures are established, much of the laboratory labor must be devoted to modification of the equipment and construction of experimental apparatus.

The appearance of one of the $SrTiO_3$ melts is shown in the photographs in Figure 9. The skull may be clearly seen at the periphery of the melt. In this experiment (2146-1) an attempt was made to nucleate crystal growth on an iridium pull-rod. A polycrystalline mass was formed which could be controlled in size and pulled. In subsequent experiments there was evidence of relatively large single crystal regions (several mm^3) that developed as the pulling proceeded. These experiments were designed to determine if pulling could be carried out at all in a skull melt. They showed that it can. This method of nucleation is unfavorable for single crystal growth. Seeding with single crystal fragments will be necessary for pulling good single crystals. Furthermore, these pulling tests were carried out quite quickly. It is expected that crystals of $SrTiO_3$ and $BaZrO_3$ will have to be pulled very slowly, as required by certain other perovskites. It should be pointed out that all melts of $SrTiO_3$ and all pulled material show evidence of partial deoxidation, even when melted under an oxygen rich atmosphere. The partial pressure of O_2 over stoichiometric $SrTiO_3$ is probably higher than one atmosphere. The resultant darkened materials are poor conductors of heat and will demand slow pulling. The two photographs in Figure 9 were made with different light attenuations. The melt is far too bright to view without a dark filter and the camera must be similarly "stopped-down". In the darker of the two pictures, dark lines or veins are evident on the top surface of the melt. The origin of such patterns,

rather characteristic of oxide melts, is speculative. In any case they serve here to show the motion caused by convective stirring of the melt. The pattern shown in the photograph is in constant and fairly rapid motion. The direction of flow, upward on the outside, toward the center, and down in the middle, is also common in melts contained in crucibles.

While pulled single crystals are the desired product, some information may be obtained from examination of solidified melts. It has not usually been possible to cool these melts sufficiently slowly to induce growth of large crystallites. Like most oxides, however, these compounds have a large volume increase on fusion and corresponding contraction on freezing. Shrinkage cavities may be formed wherein the remaining liquid may crystallize relatively slowly and without restraint. With $SrTiO_3$ melts, these growth conditions produce interesting dendritic growth patterns. The individual crystallites are small cubes showing growth hillocks. These cubes are oriented in long dendritic chains along a low index direction. This direction is frequently $\langle 100 \rangle$ but "corner growth" along $\langle 111 \rangle$ is also seen, and propagation along $\langle 110 \rangle$ may occur too. The "registry" of the crystallites may be maintained over a considerable distance. Examples of these dendritic formations are shown in the photographs in Figure 10. With $BaZrO_3$, the crystallites tend to be much smaller and are less well developed. Well formed cubes are not found, although only cubic $BaZrO_3$ may be found by x-ray analysis. These melts tend to quench more rapidly and produce fine crystallites. Unlike strontium titanate, the solidified melts of $BaZrO_3$ are not darkened but are of a cream-white color, indicating little if any reduction.

B. Physical Examination of Products:

Proof of the thesis that the lifetime of a fluorescent ion can be extended by incorporation into a cubic perovskite structure must rest on a fluorescent spectrum analysis and measurement of fluorescent decay times. In addition the absorption spectrum is highly informative. The spectrocopic information will be most valuable when it is obtained on a crystal of high purity and optical quality. The experimental spectroscopic methods demand a certain minimum quality and size of crystal. In other words,

the crystal synthesis problems must be solved before detailed physical examination is warranted. To the present, the synthesis problem has represented the major part of the program effort. Nevertheless, until quality crystals can be pulled, we must obtain what guidance and data we can from the materials so far synthesized.

All materials synthesized have been analyzed by x-ray and emission spectroscopy. In almost all cases where the composition is near stoichiometry, the only phase observed is the perovskite ($SrTiO_3$ or $BaZrO_3$). The emission spectroscopic data shows the presence of Si, Al, Mg, Ca and traces of Cu in $SrTiO_3$ and Si, Al, Ca and traces of Mg, Fe and Cu in $BaZrO_3$. It is expected that contamination can be reduced by using higher purity starting materials. When dopants have been added they have invariably been detected in the crystalline products.

A very few attempts have been made to obtain fluorescence spectra. In particular, a spectrum has been obtained for Sm doped $BaZrO_3$, made early in the program. A spectrum showing only a few well defined lines was obtained at 77°K. The spectrum will be reexamined in hope of identifying the transition. This phase of the program is quite incomplete. An attempt will be made during the coming period, to characterize all doped crystals of $BaZrO_3$ (and where desirable $SrTiO_3$).

Several crystals of $SrTiO_3$ doped with Mn, were previously synthesized by the Verneuil technique. These did not exhibit the desired fluorescence from Mn^{+4}. The valence state and location of the dopant remained in doubt. Representative samples of Mn: $SrTiO_3$ have been oriented so that they may be examined by electron spin resonance. This data will be obtained with the cooperation of Dr. Paul Kasai of the Union Carbide Corporation, Research Institute. It is anticipated that this will clarify the state of the doping in Mn: $SrTiO_3$.

C. Structure Analysis:

During the first phase of this work, experiments were run in attempts to grow several of the perovskites and refractory oxides by means of a flux technique. Several of the materials grown were identified, however, others did not

match available patterns of the compounds.

Since that time, single-crystal x-ray work has been done to identify the structures. All x-ray data were collected on a Buerger Precession Camera using Copper K_{α} radiation. The results are as follows:

ThO_2 Emission spectroscopy showed the only major cation to be Th. Samples of the material were heated to 1000°C in an oxygen atmosphere, however, no weight gain or loss was observed indicating complete oxidation of the Th. Single crystal data gave the following results:

Crystal Class - Monoclinic
Lattice Constants - a = 5.25 Å
b = 6.23 Å
c = 6.93 Å
γ = 50° 55"

UO_2 Emission spectroscopy showed U and a trace of Li. Single crystal data gave the following results:

Crystal Class - Tetragonal
Lattice Constants - a = 6.85 Å
b = 11.28 Å

$SrZrO_3$ Emission spectroscopy showed the major cations to be Sr and Zr. Examination of several crystals showed a rhombohedral habit. Single-crystal data gave the following results:

Crystal Class - Rhombohedral
Lattice Constants - a = 5.89 Å
α = 58° 34'

These data are not the same as those reported by Roth[2] for $SrZrO_3$. However he found the data on $SrTiO_3$ to be rather ambiguous. In either case, the structure is not cubic, as is $BaZrO_3$.

VI. PLANS FOR NEXT PERIOD

The program for the next period will emphasize experiments on the Czochralski pulling of $BaZrO_3$. It is hoped that the difficulties of skull-melting can be overcome well enough to produce the type of crystals needed for a good evaluation. The solution of this problem requires having a more reproducible starting procedure. Variations in the starting procedure are now being tested.

When crystals of $BaZrO_3$ can be pulled, specimens of pure $BaZrO_3$ will be made. Crystals will also be pulled from melts doped with one or more of the following rare earth oxides (Sm_2O_3, Eu_2O_3, Yb_2O_3). If the evidence indicates the presence of the trivalent state for the rare earth, experiments may be conducted in reducing atmospheres.

Materials to be made and those already made on this program will be examined to the extent feasible, with regard to crystal quality, to ascertain the state of the host crystal and dopant. When possible this will include fluorescence spectra. Emphasis will be given to determining the state of rare earth dopant ions in $BaZrO_3$. The investigation of the state of Mn: $SrTiO_3$ by electron spin resonance will be completed.

REFERENCES

(1) O. H. Nestor, Annual Summary Report, Contract Nonr-4131(00), June 25, 1964

(2) R. S. Roth, J. Res., Nat. Bureau Standards, 58 75 (1957)

(3) A. von Hippel, "Molecular Science and Engineering", Technology Press of M. I. T. and John Wiley and Sons, N. Y., 1959, p. 148

(4) F. W. Lytle, J. App. Phys. 35 2212 (1964) and references therein

(5) H. Fay, unpublished data on low temperature properties of $SrTiO_3$

(6) H. A. Eick, N. C. Baenziger, and L. Eyring, J. A. C. S. 78 5147 (1956)

(7) J. Brous, I. Frankuchen, and E. Banks, Acta. Cryst. 6 67 (1953)

(8) R. E. Grace, U. S. Atomic Energy Commission Technical Progress Report COO-359-10

(9) M. Kestigian, J. G. Dickinson and R. Ward, J. A. C. S. 79 5598 (1957)

(10) W. R. Buessem and S. R. Butler "Kinetics of High Temperature Processes", The Technology Press of M. I. T. and John Wiley and Sons, Inc., N. Y., 1959 p. 13

(11) W. R. Buessem, P. A. Marshall and S. R. Butler, Reports dated 31 July, 1958 and 1 April, 1957 Contract No. DA-36-039 Signal Corps-75036

(12) E. J. W. Verwey "Oxidic Semi-conductors" p. 151 in "Semi-conducting Materials", Butterworths, London, 1951

(13) H. P. R. Frederikse, W. R. Thurber and W. R. Hosler, Phys. Rev. 134 A 442 (1964)

(14) H. A. Johansen and J. G. Cleary, J. Electrochem. Soc. 111 100 (1964)

(15) R. W. Taylor and H. Schmalzried, J. Phys. Chem 68 2444 (1964)

(16) F. A. Kröger and H. J. Vink, Solid State Physics Vol. 3, p. 307 (1956)

(17) R. F. Schaufele and M. J. Weber, Paper C5, Am. Physical Soc. Meeting, Chicago, Oct. 1964

(18) E. M. Levin et al. "Phase Diagrams for Ceramists", The American Ceramic Society, 1956, 1959 and 1964

(19) K. Nassau and A. M. Broyer, J. Am. Ceram. Soc. 45 474 (1962)

(20) A. Linz, Crystal Physics Group, Center for Material Science and Engineering, Mass. Inst. Technology, private communication

(21) A. E. van Arkel, E. A. Flood and N. F. H. Bright, Canadian J. Chem. 31 1009 (1953)

(22) F. R. Monteforte, F. W. Swanekamp and L. G. VanUitert, J. Applied Physics 32 959 (1961)

(23) J. A. Stratton, "Electromagnetic Theory" p. 50, McGraw-Hill, New York, 1941

(24) P. G. Simpson, "Induction Heating", Chapters 1, 2 and Appendix, McGraw-Hill, New York, 1960

(25) E. Janke and F. Emde, "Tables of Functions" Chapter VIII, Dover, New York 1945

(26) R. C. McMaster, editor, "Nondestructive Testing Handbook" Vol. II, Chapters 36 and 37, The Roland Press Co., New York, 1959

(27) F. Förster and K. Stambke, Z. für Metallkunde 45 166, 171, 197, 206 and 221 (1954)

TABLE A

SUMMARY OF SKULL-MELTING EXPERIMENTS

Material	Coil	Frequency	Duration of Melt	Remarks	Ref.
$SrTiO_3$	10 turn 5" ID 3/8" tubing	310 Kc	2.5 hrs.	Melted 3 kg. "Cubes" of $SrTiO_3$ in cooled mass.	1996-44
$BaZrO_3$	10 turn 5" ID	308 Kc	1 hr.	Several starts. Attempt to cool slowly for crystals.	1996-68
$BaZrO_3$	8 turn 5" ID	319 Kc	-----	Unreacted powders. Abortive run. Spark and water leak.	1996-71
$BaZrO_3$	8, 4 and 6 turn 5" ID	8 = 321 Kc 4 = 258 Kc 6 = 258 Kc	50 min.	Tried several coils. Melt only with 6 turn before shutdown.	1996-76
$BaZrO_3$	6 turn 5" ID 6 turn 6 1/2" ID	341 Kc 321 Kc	short	Run ca. 50 min. before hole in boat. Light colored melt.	1996-78
$BaZrO_3$	6 turn 6 1/2" ID	320 Kc	nil	Several attempts to start without success.	1996-83 -86
$SrTiO_3$	10 turn 7" ID		short	Eventually burned through ceramic "bottom".	1996-90
$SrTiO_3$	10 turn 7" ID		short	Spark from coil to boat, shut down.	1996-91
$SrTiO_3$	10 turn 4 1/8" ID	390 Kc	short	Aborted due to arc on coil.	1996-92
$SrTiO_3$	8 turn 4 1/8" ID	400 Kc	short	Melt established but lost - poor coupling.	1996-94
$SrTiO_3$	5 turn 5" ID	2.44 Mc	2 hrs.	Good melt - attempt to pull (see photograph)	2146-1
$SrTiO_3$	5 turn 5" ID	2.44 Mc	4.5 hrs.	Good melt - pulled crystalalline material on Ir rod (2146-4-26)	2146-4
SrTiO3	5 turn 5" ID	2.49 Mc	short	Melt leakd out - shut down.	2146-5
$SrTiO_3$	5 turn 5" ID	ca. 2.5 Mc	1.5 hrs.	Pulled for 40 min. Eu doping (2146-6-24)	2146-6

TABLE A (Continued)

Material	Coil	Frequency	Duration of Melt	Remarks	Ref.
$SrTiO_3$	5 turn 5" ID	"	----	Tried to restart previous run, unsuccessful.	2146-8
$SrTiO_3$	5 turn 5" ID	"	7 hrs.	Pulled crystalline material (2146-9-26)	2146-9
$SrTiO_3$		"	3 hrs.	Melted on top of previous run - pulled material.	2146-11
$BaZrO_3$	5 turn 5 1/2" ID	"	3 hrs.	Stable melt of $BaZrO_3$. Attempt to pull material on ZrO_2 rod not successful.	2146-12
$BaZrO_3$		"	short	Melt too low-lost coupling.	2146-13
$SrTiO_3$	5 turn 6" ID	"	5 hrs.	Good melt. Attempt to pull on seed. Testing control.	2146-15
$SrTiO_3$	5 turn 5" ID	2.67 Mc	5 hrs.	Shielded Coil-Plate current control. Attempt to pull - lost due to setting current too low.	2146-41
$BaZrO_3$	5 turn 5" ID	2.87 Mc	short	Short run due to gas entrapment. Melt forced out violently - Aborted.	2146-51

FIGURE 1

PHASE DIAGRAMS

SrO–TiO_2

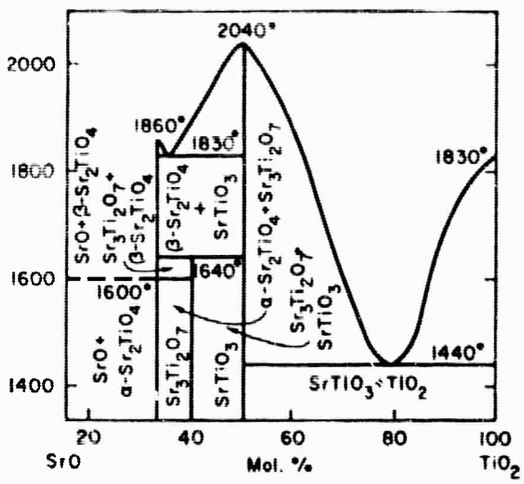

FIG. 297.—System SrO–TiO_2.

Miroslawa Dryś and Włodzimierz Trzebiatowski, *Roczniki Chem.*, **31**, 492 (1957).

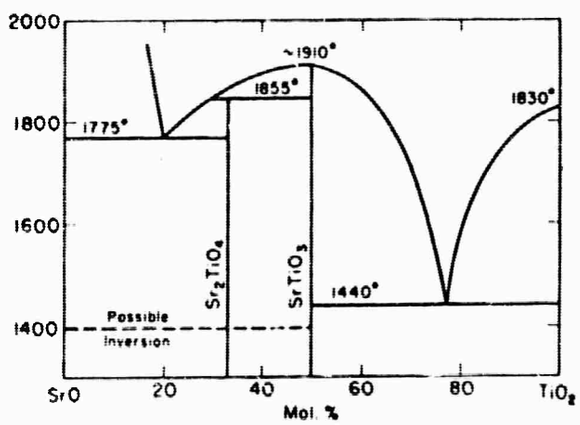

FIG. 298.—System SrO–TiO_2; tentative.

Rustum Roy; private communication, 1957.

ZrO_2–RO

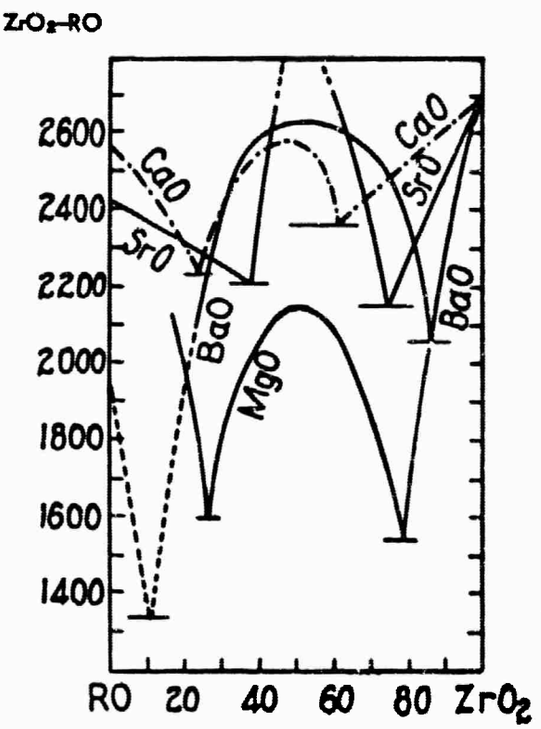

FIG. 147.—Melting curves of BaO–ZrO_2, CaO–ZrO_2, MgO–ZrO_2, and SrO–ZrO_2.

H. von Wartenberg and W. Gurr, *Z. anorg. u. allgem. Chem.*, 196, 381 (1931).

Taken from reference (18)

FIGURE 2

COMPLEX EFFECTIVE PERMEABILITY

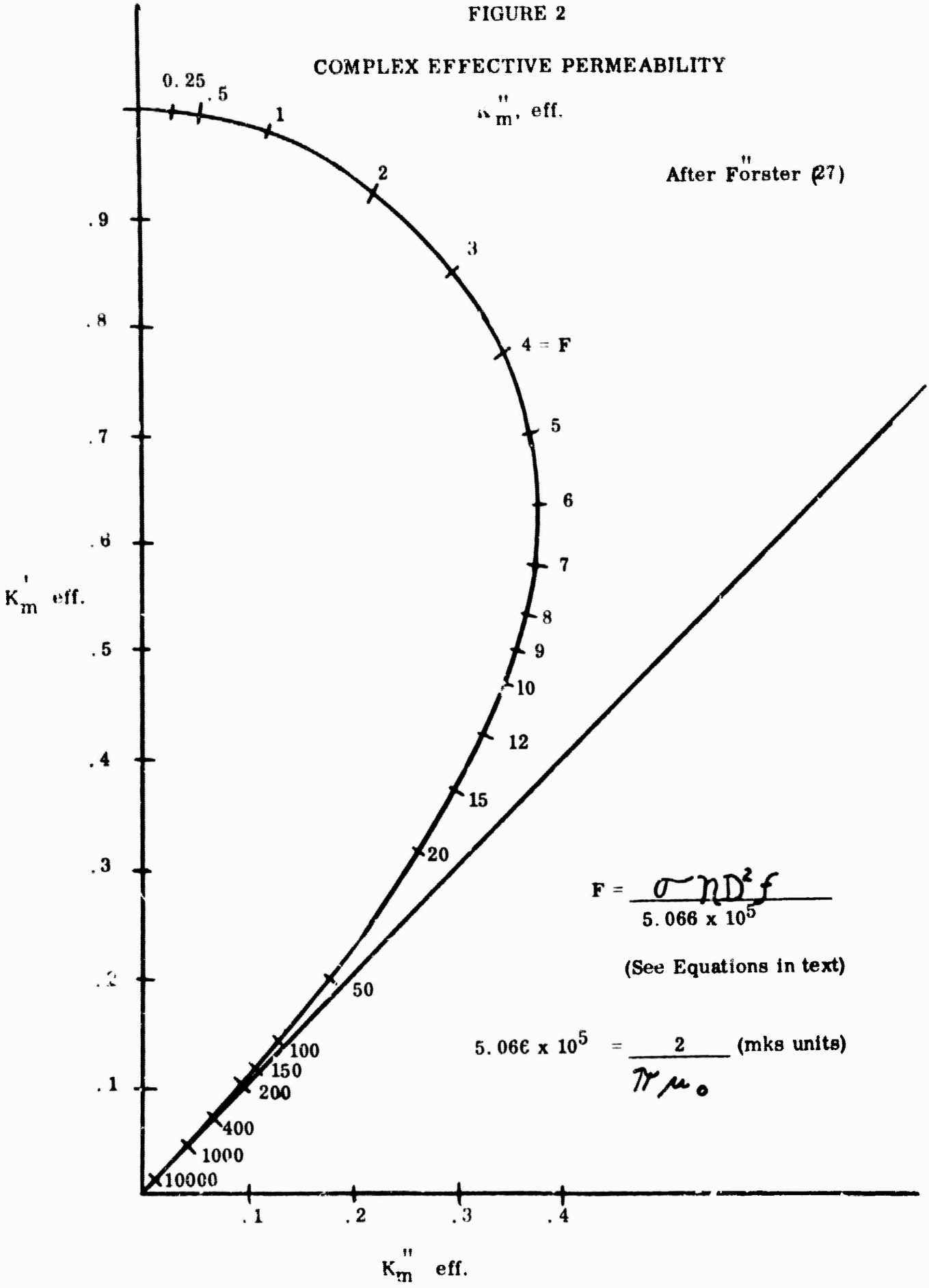

$$F = \frac{\sigma \eta D^2 f}{5.066 \times 10^5}$$

(See Equations in text)

$$5.066 \times 10^5 = \frac{2}{\pi \mu_o} \text{ (mks units)}$$

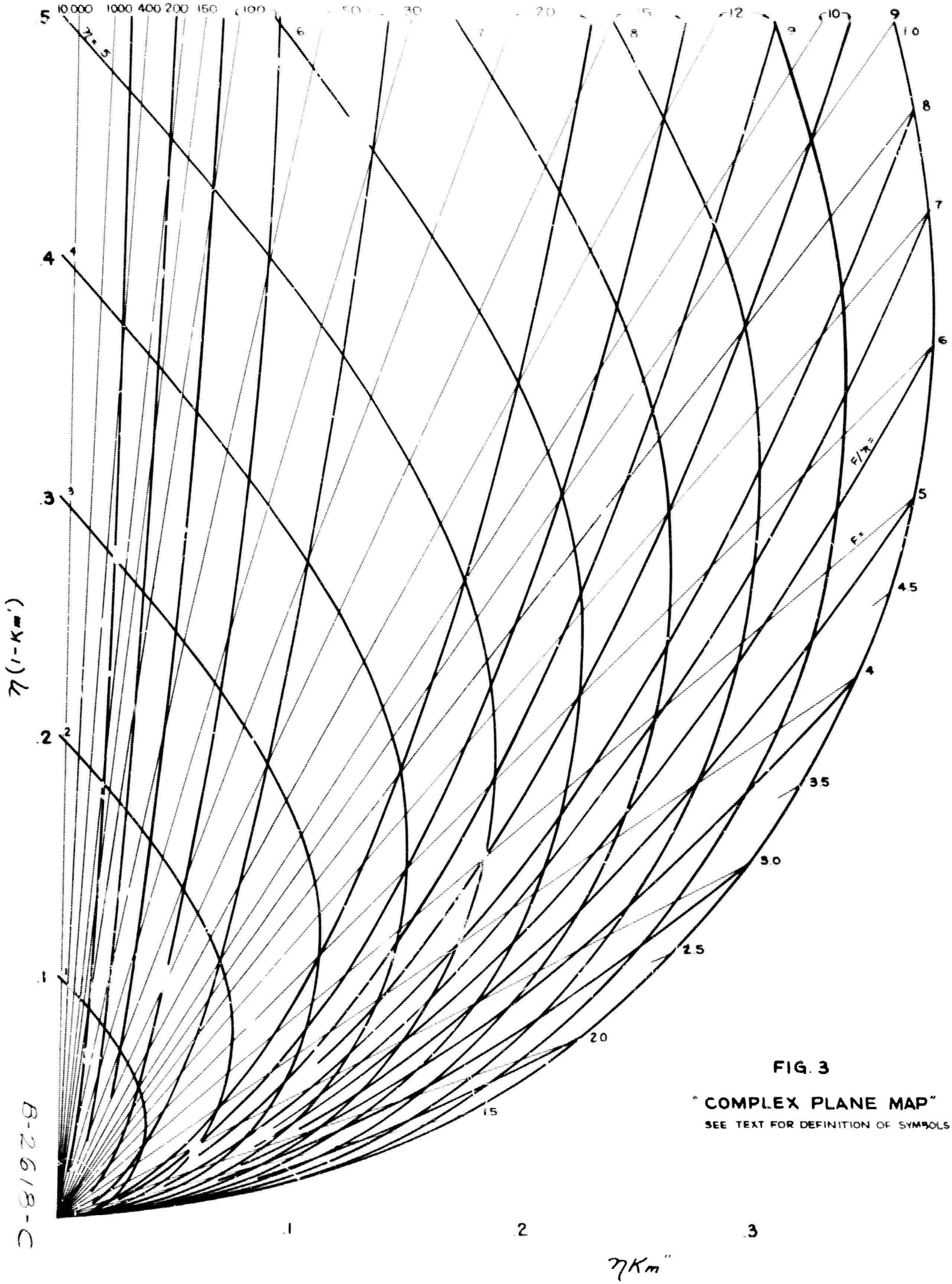

FIG. 3

"COMPLEX PLANE MAP"

SEE TEXT FOR DEFINITION OF SYMBOLS

C-2618-6

FIGURE 4

ELECTRICAL CONDUCTIVITIES OF VARIOUS SUBSTANCES

AS A FUNCTION OF 1/T °K

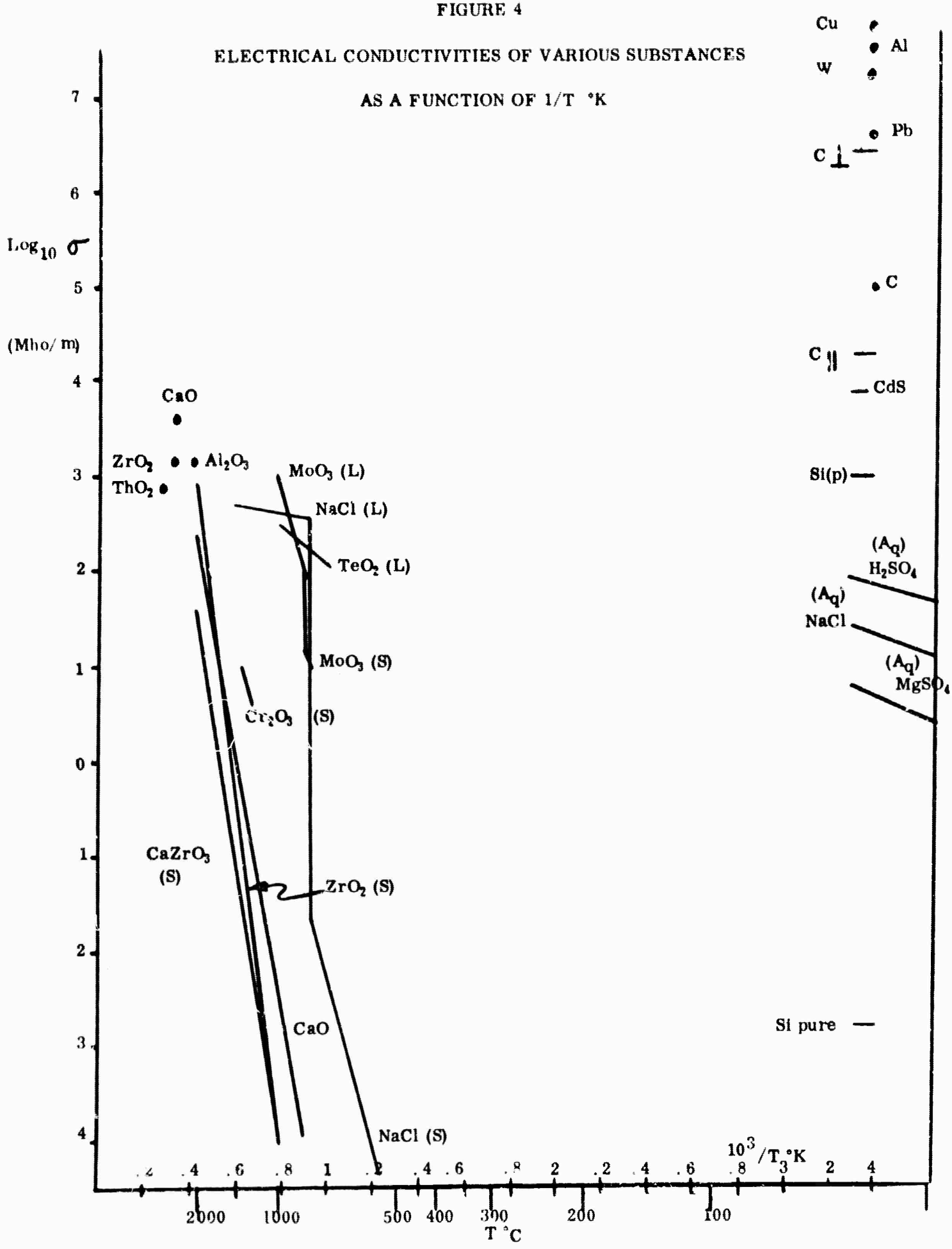

FIGURE 5

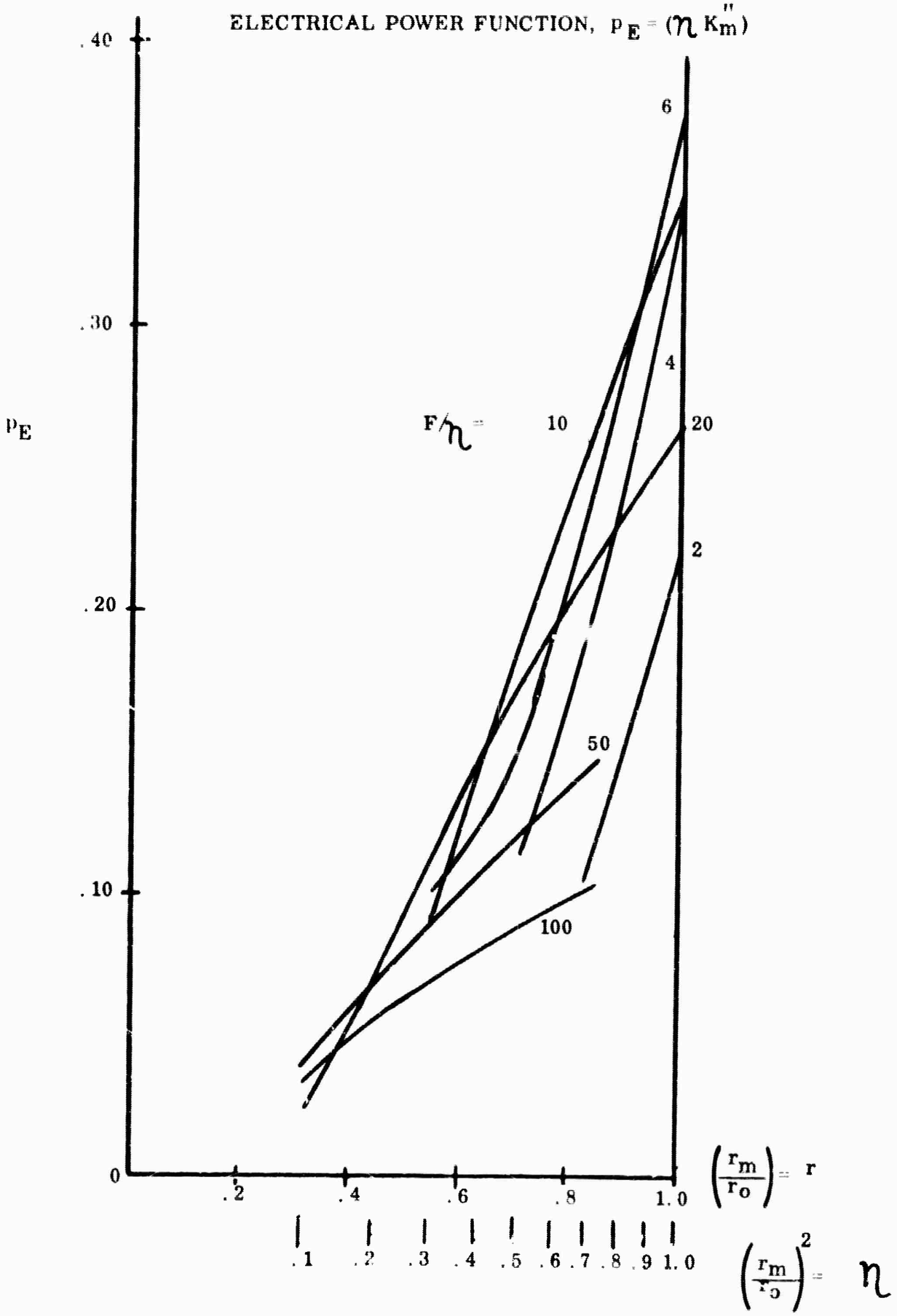
ELECTRICAL POWER FUNCTION, $p_E = (\eta K_m'')$
.40
.30
.20
.10
0
p_E
F/η =
6
4
10
20
2
50
100
.2
.4
.6
.8
1.0
$\left(\frac{r_m}{r_o}\right)$ = r
.1
.2
.3
.4
.5
.6
.7
.8
.9
1.0
$\left(\frac{r_m}{r_o}\right)^2$ = η

FIGURE 6

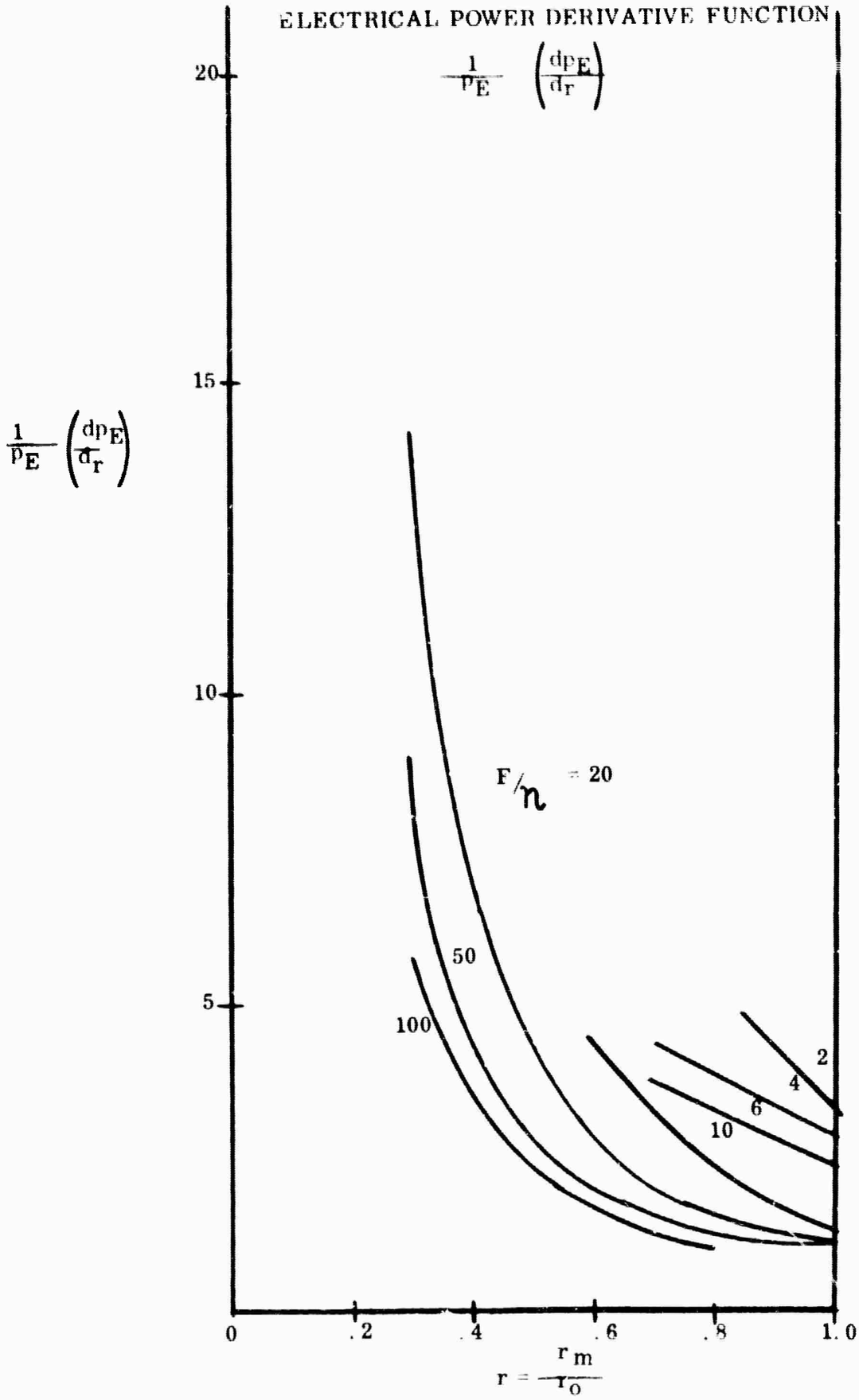
ELECTRICAL POWER DERIVATIVE FUNCTION
$\frac{1}{p_E}\left(\frac{dp_E}{dr}\right)$
20
15
10
5
0
.2
.4
.6
.8
1.0
F/η = 20
50
100
2
4
6
10
$r = \frac{r_m}{r_o}$

FIGURE 7

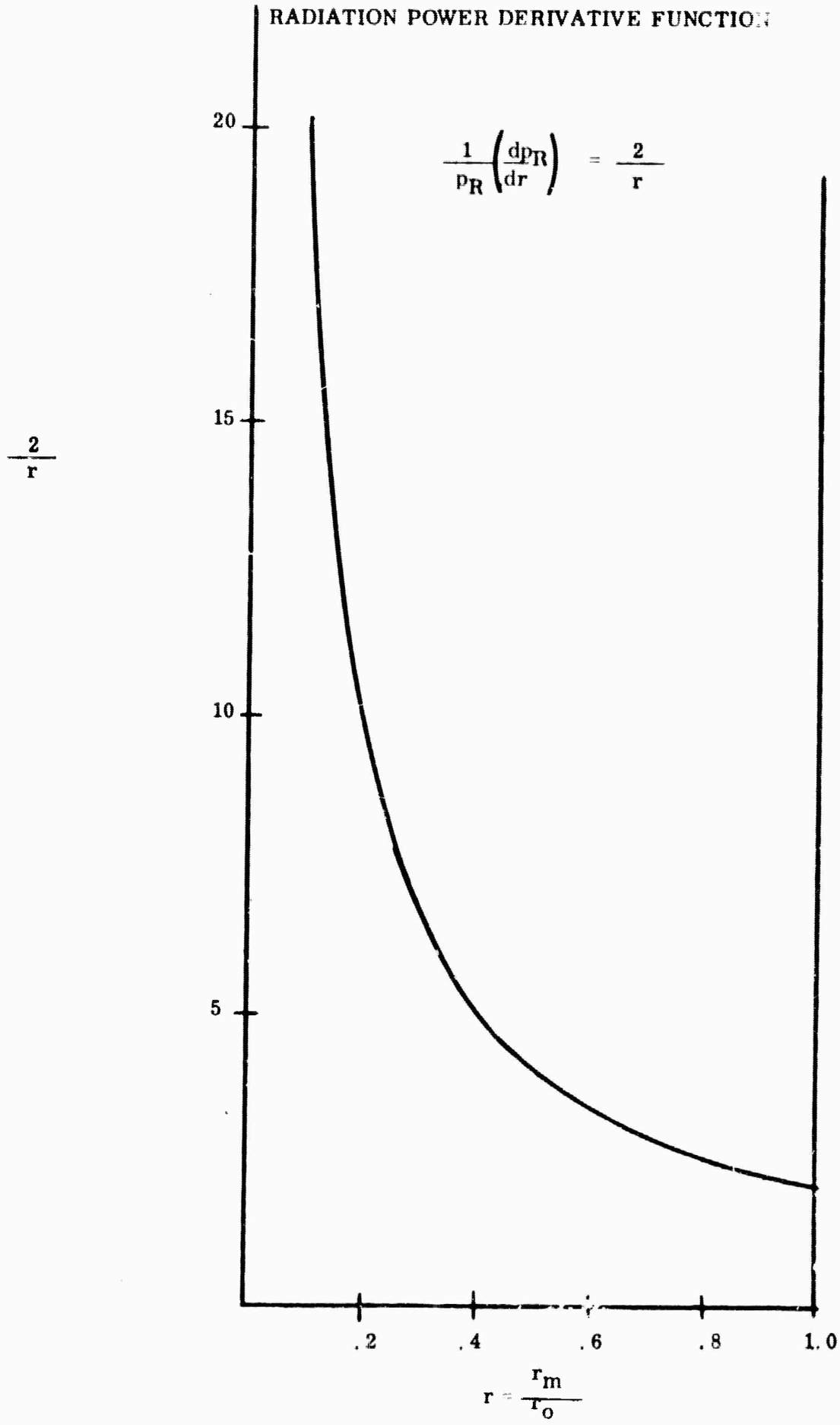
RADIATION POWER DERIVATIVE FUNCTION
$\frac{1}{p_R}\left(\frac{dp_R}{dr}\right) = \frac{2}{r}$
20
15
10
5
$\frac{2}{r}$
.2
.4
.6
.8
1.0
$r = \frac{r_m}{r_o}$

FIGURE 8

THERMAL CONDUCTIVITY

POWER DERIVATIVE FUNCTION

$$\frac{1}{p_T}\left(\frac{d\,p_T}{dr}\right) = \frac{p_T}{r}$$

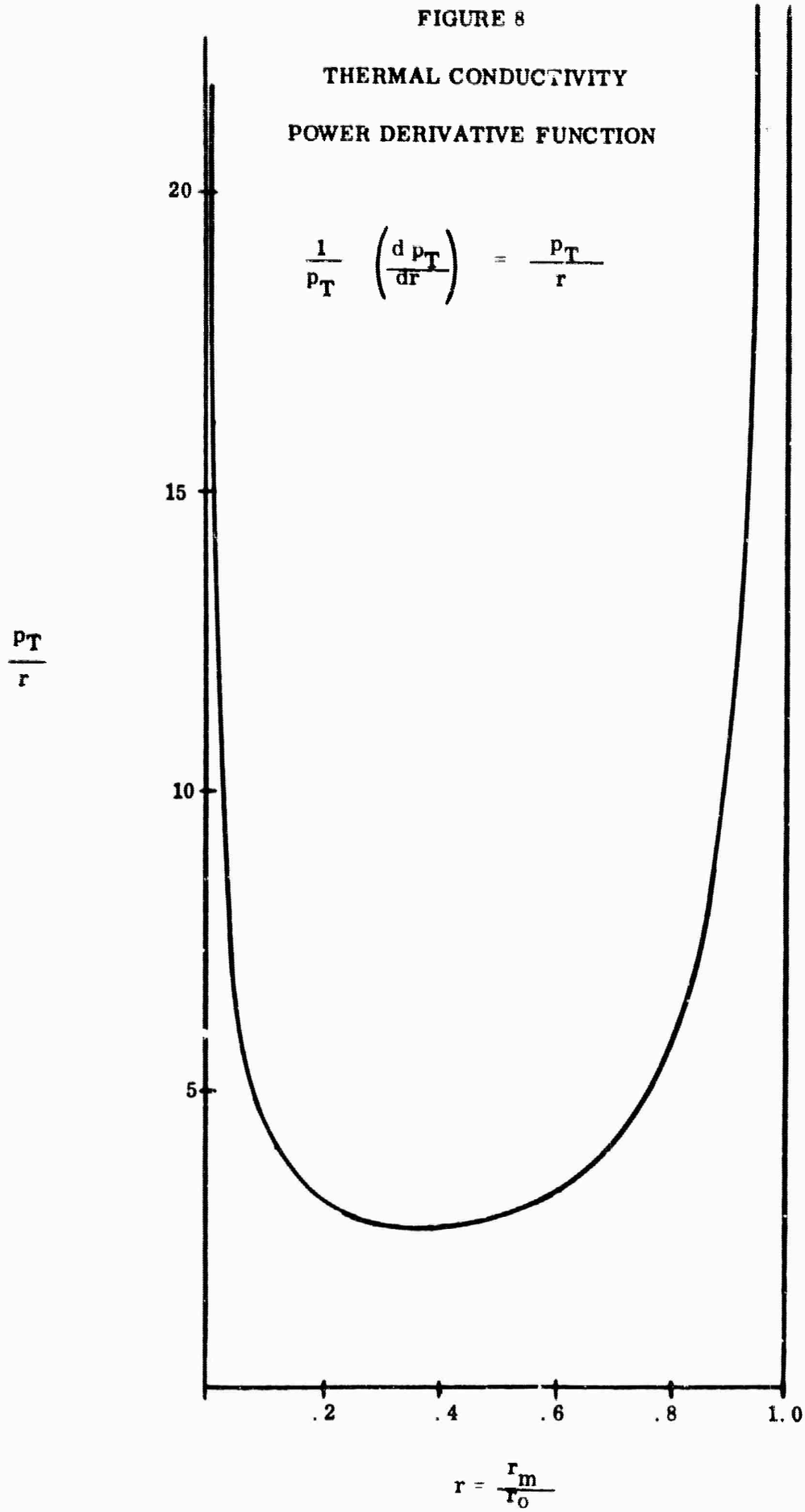

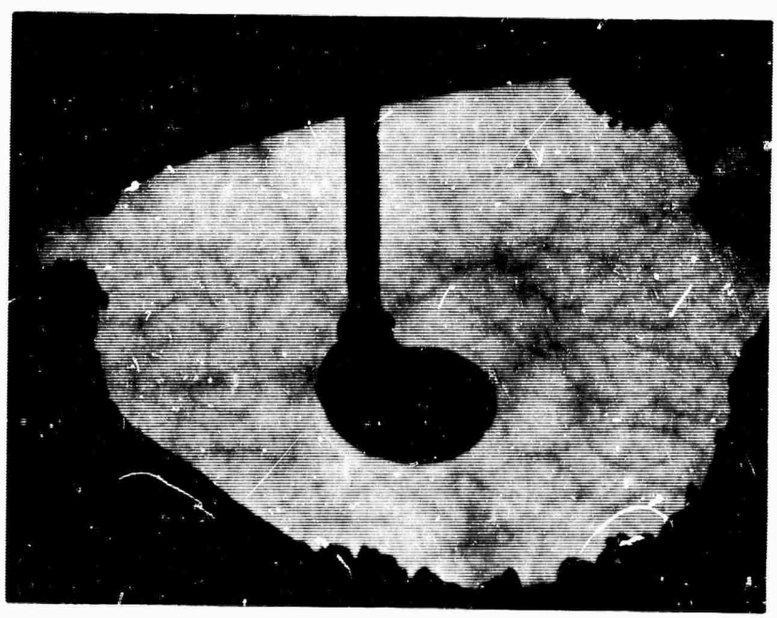

Figure 9 - Photographs of Skull Melts of $SrTiO_3$

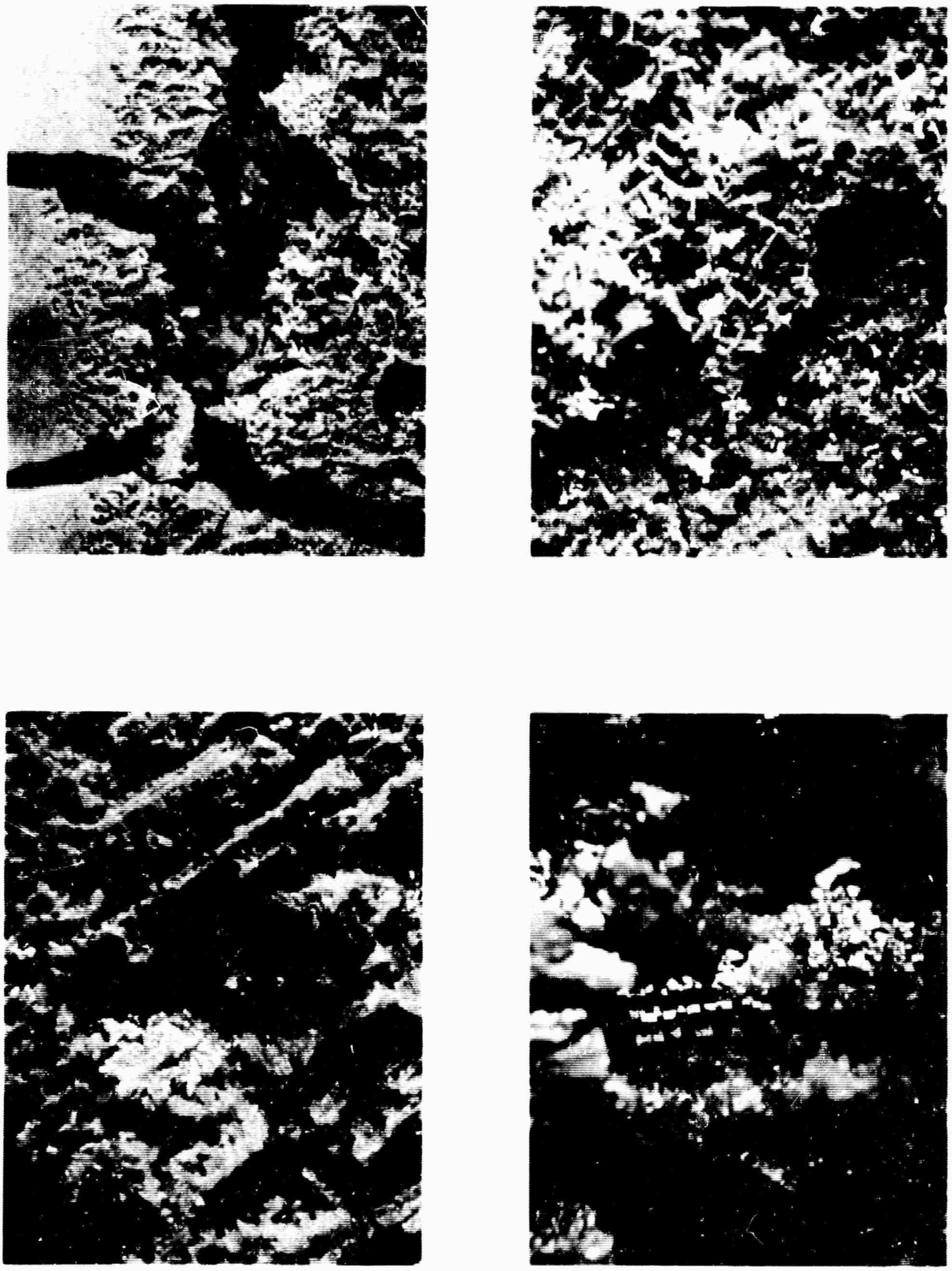

Figure 10 - Photographs of Solidified Melts of $SrTiO_3$
Showing Dendritic Growth

1	0030	R. S. CONGLETON	54
2	0030	HUGHES AIRCRAFT CORP.	54
3	0030	AEROSPACE GROUP	54
4	0030	RESEARCH & DEVELOPMENT DIVISION	54
5	0030	CULVER CITY, CALIFORNIA	54
1	0035	BASIL CURNUTTE, JR.	54
2	0035	KANSAS STATE UNIVERSITY	54
3	0035	MANHATTAN, KANSAS	54
1	0042	G. H. DIEKE	54
2	0042	JOHNS HOPKINS UNIVERSITY	54
3	0042	BALTIMORE 18, MARYLAND	54
1	0092	C. H. KELLER	54
2	0092	PEK LABS, INC.	54
3	0092	925 EVELYN AVENUE	54
4	0092	SUNNYVALE, CALIFORNIA	54
1	0093	S. P. KELLER	54
2	0093	INTERNATIONAL BUSINESS MACHINES	54
3	0093	T. J. WATSON RESEARCH CENTER	54
4	0093	YORKTOWN HEIGHTS, NEW YORK	54
1	0108	A. LEMPICKI	54
2	0108	GENERAL TELEPHONE & ELECTRONICS LABS	54
3	0108	BAYSIDE 60, NEW YORK	54

1	0117	R. C. PASTOR	54
2	0117	KORAD CORPORATION	54
3	0117	2520 COLORADO AVENUE	54
4	0117	SANTA MONICA, CALIFORNIA	54
1	0121	T. C. MCAVOY	54
2	0121	CORNING GLASS WORKS	54
3	0121	CORNING, NEW YORK	54
1	0122	W. MCKUSICK	54
2	0122	EASTMAN KODAK COMPANY	54
3	0122	APPARATUS AND OPTICAL DIVISION	54
4	0122	400 PLYMOUTH AVENUE, N.	54
5	0122	ROCHESTER 4, NEW YORK	54
1	0139	O. H. NESTOR	54
2	0139	LINDE COMPANY	54
3	0139	1500 POLCO STREET	54
4	0139	INDIANAPOLIS 24, INDIANA	54
1	0144	J. W. NIELSON	54
2	0144	AIRTRON, A DIVISION OF LITTON INDUSTRIES	54
3	0144	200 EAST HANOVER AVENUE	54
4	0144	MORRIS PLAINS, NEW JERSEY	54
1	0148	GERALD OSTER	54
2	0148	CHEMISTRY DEPARTMENT	54
3	0148	POLYTECHNIC INSTITUTE OF BROOKLYN	54
4	0148	333 JAY STREET	54
5	0148	BROOKLYN 1, NEW YORK	54

1	0178	DAVID STOCKMAN	54
2	0178	ELECTRONICS LABORATORY	54
3	0178	GENERAL ELECTRIC COMPANY	54
4	0178	SYRACUSE, NEW YORK	54

1	0189	J. W. TURNER	54
2	0189	WESTINGHOUSE ELECTRIC CORP.	54
3	0189	ELECTRONICS DIVISION	54
4	0189	P. O. BOX 1897	54
5	0189	BALTIMORE 3, MARYLAND	54

1	0207	R. W. YOUNG	54
2	0207	AMERICAN OPTICAL COMPANY	54
3	0207	SOUTHBRIDGE, MASSACHUSETTS	54

1	0213	DR. JERALD R. IZATT	54
2	0213	NEW MEXICO STATE UNIVERSITY	54
3	0213	UNIVERSITY PARK, NEW MEXICO	54

1	0214	PROFESSOR A. K. KAMAL	54
2	0214	PURDUE UNIVERSITY	54
3	0214	SCHOOL OF ELECTRICAL ENGINEERING	54
4	0214	LAFAYETTE, INDIANA	54
1	0215	MR. THOMAS C. MARSHALL	54
2	0215	COLUMBIA UNIVERSITY	54
3	0215	DEPT. OF ELECTRICAL ENGINEERING	54
4	0215	NEW YORK 27, NEW YORK	54
1	0216	MR. CHARLES G. NAIMAN	54
2	0216	MITHRAS, INC.	54
3	0216	CAMBRIDGE 39, MASSACHUSETTS	54
1	0217	DR. J. H. SCHULMAN	54
2	0217	SOLID STATE DIVISION	54
3	0217	U. S. NAVAL RESEARCH LABORATORY	54
4	0217	WASHINGTON 25, D. C.	54
1	0218	DR. JACK A. SOULES	54
2	0218	PHYSICS DEPARTMENT P.O. Box 818	54
3	0218	NEW MEXICO STATE UNIVERSITY 88070	54
4	0218	UNIVERSITY PARK, NEW MEXICO.	54
1	0219	DR. ARDEN SHER	54
2	0219	VARIAN ASSOCIATES	54
3	0219	611 HANSEN WAY	54
4	0219	PALO ALTO, CALIFORNIA	54

1	0220	PHYSICAL SCIENCES DIVISION	54
2	0220	ARMY RESEARCH OFFICE	54
3	0220	OFFICE, CHIEF, RESEARCH & DEVELOPMENT	54
4	0220	WASHINGTON 25, D. C.	54
5	0220	ATTN DR. ROBERT A. WATSON	54
1	0221	CHIEF SCIENTIST	54
2	0221	U. S. ARMY ELECTRONICS COMMAND	54
3	0221	FORT MONMOUTH, NEW JERSEY	54
4	0221	ATTN DR. HANS K. ZIEGLER	54
1	0222	DIRECTOR, INSTITUTE FOR EXPLATORY RESEARCH	54
2	0222	ARMY SIGNAL RESEARCH&DEVELOPMENT LABORATORY	54
3	0222	FORT MONMOUTH, NEW JERSEY	54
4	0222	ATTN DR. E. M. REILLEY	54
1	0223	ASST DIRECTOR OF SURVEILLANCE	54
2	0223	ARMY SIGNAL RESEARCH&DEVELOPMENT LABORATORY	54
3	0223	FORT MONMOUTH, NEW JERSEY	54
4	0223	ATTN DR. HARRISON J. MERRILL	54
1	0225	DIRECTOR OF RESEARCH & DEVELOPMENT	54
2	0225	ARMY ORDNANCE MISSILE COMMAND	54
3	0225	HUNTSVILLE, ALABAMA	54
4	0225	ATTN MR. WILLIAM D. MCKNIGHT	54

1	0226	OFFICE, CHIEF OF NAVAL OPERATIONS /OP-07T-1/		54
2	0226	DEPARTMENT OF THE NAVY		54
3	0226	WASHINGTON 25, D. C.		54
4	0226	ATTN MR. BEN ROSENBERG		54
1	0227	BURFAU OF NAVAL WEAPONS /RR-2/		54
2	0227	DEPARTMENT OF THE NAVY		54
3	0227	WASHINGTON 25, D. C.		54
4	0227	ATTN DR. C. H. HARRY		54
1	0228	BUREAU OF SHIPS /CODE 305/		54
2	0228	DEPARTMENT OF THE NAVY		54
3	0228	WASHINGTON 25, D. C.		54
4	0228	ATTN DR. G. C. SPONSLER		54
1	0229	OFFICE OF NAVAL RESEARCH /CODE 402C/		54
2	0229	DEPARTMENT OF THE NAVY		54
3	0229	WASHINGTON 25, D. C.		54
4	0229	ATTN DR. SIDNEY REED		54
1	0230	OFFICE OF NAVAL RESEARCH /CODE 421/	03 COPIES	54
2	0230	DEPARTMENT OF THE NAVY		54
3	0230	WASHINGTON 25, D. C.		54
4	0230	ATTN MR. FRANK B. ISAKSON		54
1	0231	OFFICE OF NAVAL RESEARCH /CODE 406T/		54
2	0231	DEPARTMENT OF THE NAVY		54
3	0231	WASHINGTON 25, D. C.		54
4	0231	ATTN MR. J. W. SMITH		54

1	0232	NAVAL RESEARCH LABORATORY /CODE 6440/	54
2	0232	DEPARTMENT OF THE NAVY	54
3	0232	WASHINGTON 25, D. C.	54
4	0232	ATTN DR. C. C. KLICK	54
1	0233	NAVAL RESEARCH LABORATORY /CODE 7360/	54
2	0233	DEPARTMENT OF THE NAVY	54
3	0233	WASHINGTON 25, D. C.	54
4	0233	ATTN DR. L. F. DRUMMETER	54
1	0234	HEADQUARTERS USAF /AFRDR-NU-3/	54
2	0234	DEPARTMENT OF THE AIR FORCE	54
3	0234	WASHINGTON, D. C.	54
4	0234	ATTN LTCOL E. N. MYERS	54
1	0235	RESEARCH & TECHNOLOGY DIVISION	54
2	0235	BOLLING AFB	54
3	0235	WASHINGTON, D. C.	54
4	0235	ATTN MR. ROBERT FEIK	54
1	0236	OFFICE, AEROSPACE RESEARCH /MROSP/	54
2	0236	WASHINGTON 25, D. C.	54
3	0236	ATTN LT. COL. IVAN ATKINSON	54
1	0238	TECHNICAL AREA MANAGER /760A/	54
2	0238	ADVANCED WEAPONS AERONAUTICAL SYSTEMS DIV	54
3	0238	WRIGHT-PATTERSON AFB	54
4	0238	OHIO	54
5	0238	ATTN MR. DON NEWMAN	54

1	0239	PROJECT ENGINEER /5237/	54
2	0239	AEROSPACE RADIATION WEAPONS	54
3	0239	AERONAUTICAL SYSTEMS DIVISION	54
4	0239	WRIGHT-PATTERSON AFB	54
5	0239	OHIO	54
6	0239	ATTN MR. DON LEWIS	54
1	0240	AIR FORCE SPECIAL WEAPONS CENTER /SWRPA/	54
2	0240	KIRTLAND AFB	54
3	0240	NEW MEXICO	54
4	0240	ATTN CAPT. MARVIN ATKINS	54
1	0241	PROJECT ENGINEER /5561/ COMET	54
2	0241	ROME AIR DEVELOPMENT CENTER	54
3	0241	GRIFFISS AFB	54
4	0241	NEW YORK	54
5	0241	ATTN MR. PHILLIP SANDLER	54
1	0242	DEPARTMENT OF ELECTRICAL ENGINEERING	54
2	0242	NEW YORK UNIVERSITY	54
3	0242	UNIVERSITY HEIGHTS	54
4	0242	NEW YORK, NEW YORK	54
5	0242	ATTN MR. THOMAS HENION	54
1	0243	BMDR 8 COPIES	54
2	0243	ROOM 2 B 263	54
3	0243	THE PENTAGON	54
4	0243	WASHINGTON 25, D. C.	54
5	0243	ATTN LT.COL. W. B. LINDSAY	54

1	0284	MR. JOHN EMMETT	54
2	0284	PHYSICS DEPARTMENT	54
3	0284	STANFORD UNIVERSITY	54
4	0284	PALO ALTO, CALIF.	54

1	0326	SECRETARY, SPECIAL GROUP ON OPTICAL MASERS	03 COPIES	54
2	0326	ODDRCE ADVISORY GROUP ON ELECTRON DEVICES		54
3	0326	346 BROADWAY - 8TH FLOOR		54
4	0326	NEW YORK 13, NEW YORK		54

1	0352	ASD /ASRCE-31/	54
2	0352	WRIGHT-PATTERSON AFB, OHIO	54

1	0354	DR. W. HOLLOWAY	54
2	0354	SPERRY RAND RESEARCH CENTER	54
3	0354	SUDBURY, MASSACHUSETTS	54

1	0372	TECHNICAL AREA MANAGER /760B/		54
2	0372	SURVEILLANCE ELECTRONIC SYSTEMS DIVISION		54
3	0372	L. G. HANSCOM AFB		54
4	0372	MASSACHUSETTS		54
5	0372	ATTN MAJOR H. I. JONES, JR.		54
1	0388	COMMANDING OFFICER		54
2	0388	U. S. NAVAL ORDNANCE LABORATORY		54
3	0388	CORONA, CALIF.		54
1	0420	DIRECTOR		54
2	0420	U. S. ARMY ENGINEERING RESEARCH		54
3	0420	AND DEVELOPMENT LABORATORIES		54
4	0420	FORT BELVOIR, VIRGINIA		54
5	0420	ATTN TECHNICAL DOCUMENTS CENTER		54
1	0449	OFFICE OF THE DIRECTOR OF DEFENSE	02 COPIES	54
2	0449	DEFENSE RESEARCH AND ENGINEERING		54
3	0449	INFORMATION OFFICE LIBRARY BRANCH		54
4	0449	PENTAGON BUILDING		54
5	0449	WASHINGTON 25, D. C.		54
1	0471	U. S. ARMY RESEARCH OFFICE	02 COPIES	54
2	0471	BOX CM, DUKE STATION		54
3	0471	DURHAM, NORTH CAROLINA		54

1	0499	DEFENSE DOCUMENTATION CENTER	20 COPIES	54
2	0499	CAMERON STATION BUILDING		54
3	0499	ALEXANDRIA 14, VIRGINIA		54
1	0527	DIRECTOR	06 COPIES	54
2	0527	U. S. NAVAL RESEARCH LABORATORY		54
3	0527	TECHNICAL INFORMATION OFFICER		54
4	0527	CODE 2000, CODE 2021		54
5	0527	WASHINGTON 25, D. C.		54
1	0555	COMMANDING OFFICER		54
2	0555	OFFICE OF NAVAL RESEARCH BRANCH OFFICE		54
3	0555	~~230 N. MICHIGAN AVENUE~~ 219 S. Dearborn		54
4	0555	CHICAGO, ILLINOIS 60604		54
1	0584	COMMANDING OFFICER		54
2	0584	OFFICE OF NAVAL RESEARCH BRANCH OFFICE		54
3	0584	207 W. 24TH ST.		54
4	0584	NEW YORK 11, NEW YORK 10011		54
1	0640	COMMANDING OFFICER		54
2	0640	OFFICE OF NAVAL RESEARCH BRANCH OFFICE		54
3	0640	1000 GEARY STREET		54
4	0640	SAN FRANCISCO, CALIFORNIA 94109		54
1	0696	AIR FORCE OFFICE OF SCIENTIFIC RESEARCH		54
2	0696	WASHINGTON 25, D. C.		54

1	0724	DIRECTOR	54
2	0724	NATIONAL BUREAU OF STANDARDS	54
3	0724	WASHINGTON 25, D. C.	54
1	0752	DIRECTOR	54
2	0752	RESEARCH DEPARTMENT	54
3	0752	U. S. NAVAL ORDNANCE LABORATORY	54
4	0752	WHITE OAK, SILVER SPRING, MD.	54
1	0780	COMMANDING OFFICER	54
2	0780	OFFICE OF NAVAL RESEARCH BRANCH OFFICE	54
3	0780	1030 EAST GREEN STREET	54
4	0780	PASADENA, CALIFORNIA 91101	54
1	0808	COMMANDING OFFICER	54
2	0808	OFFICE OF NAVAL RESEARCH BRANCH OFFICE	54
3	0808	495 SUMMER STREET	54
4	0808	BOSTON ~~10~~, MASS. 02210	54
1	0836	U. S. NAVAL RADIOLOGICAL DEFENSE LABORATORY	54
2	0836	/CODE 941/	54
3	0836	SAN FRANCISCO, CALIFORNIA 94135	54
1	0853	COMMANDING OFFICER	54
2	0853	U. S. ARMY MATERIALS RESEARCH AGENCY	54
3	0853	ATTN TECHNICAL LIBRARY	54
4	0853	WATERTOWN, MASSACHUSETTS 02172	54

1	0875	BOULDER LABORATORIES	54
2	0875	NATIONAL BUREAU OF STANDARDS	54
3	0875	ATTN LIBRARY	54
4	0875	BOULDER, COLORADO	54
1	0918	AIR FORCE WEAPONS LABORATORY	54
2	0918	ATTN GUENTHER WLRPF	54
3	0918	KIRTLAND AIR FORCE BASE	54
4	0918	NEW MEXICO	54
1	0932	CHIEF, BUREAU OF NAVAL WEAPONS	54
2	0932	DEPARTMENT OF THE NAVY	54
3	0932	WASHINGTON 25, D. C.	54
4	0932	ATTN J. M. LEE RMGA-81	54
1	0976	AIR FORCE CAMBRIDGE RESEARCH LABORATORIES	54
2	0976	ATTN CRXL-R, RESEARCH LIBRARY	54
3	0976	LAWRENCE G. HANSCOM FIELD	54
4	0976	BEDFORD, MASSACHUSETTS	54
1	0988	BATTELLE MEMORIAL INSTITUTE	54
2	0988	505 KING AVENUE	54
3	0988	COLUMBUS 1, OHIO	54
4	0988	ATTN BMI-DEFENDER	54
1	1030	HEADQUARTERS, USAELRDL	54
2	1030	FORT MONMOUTH, NEW JERSEY 07703	54
3	1030	ATTN SELRA/SAR,NO-4, X, AND PF	54

1	1032	COMMANDER, U. S. NAVAL ORDNANCE TEST STATION	54
2	1032	CHINA LAKE, CALIF	54
3	1032	ATTN MR. G. A. WILKINS /CODE 4041/	54
1	1036	J. C. ALMASI	54
2	1036	GENERAL ELECTRIC COMPANY	54
3	1036	ADVANCED TECHNOLOGY LABORATORIES	54
4	1036	SCHNECTADY, N. Y.	54
1	1039	PROF. RUBIN BRAUNSTEIN	54
2	1039	UNIVERSITY OF CALIFORNIA	54
3	1039	DEPARTMENT OF PHYSICS	54
4	1039	LOS ANGELES 24, CAL.	54
1	1040	N. I. ADAMS	54
2	1040	PERKIN-ELMER CORP.	54
3	1040	NORWALK, CONN.	54
1	1046	E. P. REIDEL	54
2	1046	QUANTUM ELECTRONICS DEPT.	54
3	1046	WESTINGHOUSE ELECTRIC CORP.	54
4	1046	RESEARCH LABORATORIES	54
5	1046	PITTSBURGH, PA.	54

1	1047	PROF. H. G. HANSON	54
2	1047	UNIVERSITY OF MINNESOTA	54
3	1047	DULUTH, MINN	54
1	1048	P. SCHAFFER	54
2	1048	LEXINGTON LABORATORIES, INC.	54
3	1048	84 SHERMAN ST.	54
4	1048	CAMBRIDGE, MASS.	54
1	1049	L. E. RAUTIOLA	54
2	1049	LINDE COMPANY, DIVISION OF UNION CARBIDE	54
3	1049	EAST CHICAGO, IND.	54
1	1050	F. S. GALASSO	54
2	1050	UNITED AIRCRAFT CORP RESEARCH LABS.	54
3	1050	400 MAIN ST.	54
4	1050	EAST HARTFORD, CONN.	54
1	1051	J. W. NIELSON	54
2	1051	AIRTRON, DIVISION OF LITTON INDUSTRIES	54
3	1051	MORRIS PLAINS, N. J.	54
1	1052	E. M. FLANIGEN	54
2	1052	LINDE COMPANY	54
3	1052	DIVISION OF UNION CARBIDE	54
4	1052	TONAWANDA, N. Y.	54

1	1053	W. PRINDLE	54
2	1053	AMERICAN OPTICAL COMPANY	54
3	1053	14 MECHANIC ST.	54
4	1053	SOUTHBRIDGE, MASS.	54
1	1054	R. G. MEYERLAND	54
2	1054	PLASMA PHYSICS	54
3	1054	UNITED AIRCRAFT CORP.	54
4	1054	EAST HARTFORD 8, CONN.	54
1	1055	PROF. N. BLOEMBERGEN	54
2	1055	HARVARD UNIVERSITY	54
3	1055	DIVISION OF ENGINEERING & APPLIED PHYSICS	54
4	1055	CAMBRIDGE 38, MASS.	54
1	1056	PROF. R. J. COLLINS	54
2	1056	UNIVERSITY OF MINNESOTA	54
3	1056	DEPARTMENT OF ELECTRICAL ENG.	54
4	1056	MINNEAPOLIS 14, MINN.	54
1	1057	DR. ALAN KOLB	54
2	1057	U. S. NAVAL RESEARCH LAB.	54
3	1057	WASHINGTON, D. C.	54
1	1058	PROF. J. M. FELDMAN	54
2	1058	CARNEGIE INSTITUTE OF TECHNOLOGY	54
3	1058	DEPARTMENT OF ELECTRICAL ENGR.	54
4	1058	PITTSBURGH 13, PENNA.	54

1	1059	PROF. ARTHUR SCHAWLOW	54
2	1059	STANFORD UNIVERSITY	54
3	1059	STANFORD, CALIFORNIA	54
1	1065	RESEARCH MATERIALS INFORMATION CENTER	54
2	1065	OAK RIDGE NATIONAL LABORATORY	54
3	1065	POST OFFICE BOX X	54
4	1065	OAK RIDGE, TENN. 37831	54
1	1066	J-5 PLANS AND POLICY DIRECTORATE	54
2	1066	JOINT CHIEFS OF STAFF	54
3	1066	REQUIREMENTS AND DEVELOPMENT DIVISION	54
4	1066	ATTN SPECIAL PROJECTS BRANCH	54
5	1066	ROOM 2D982, THE PENTAGON	54
6	1066	WASHINGTON, D. C., 20301	54
1	1067	ADVANCED RESEARCH PROJECTS AGENCY	54
2	1067	RESEARCH AND DEVELOPEMENT FIELD UNIT	54
3	1067	APO 143, BOX 41	54
4	1067	SAN FRANCISCO, CALIF.	54
1	1068	ADVANCED RESEARCH PROJECTS AGENCY	54
2	1068	RESEARCH & DEVELOPMENT FIELD UNIT	54
3	1068	APO 146, BOX 271	54
4	1068	SAN FRANCISCO, CALIFORNIA	54
5	1068	ATTN MR. TOM BRUNDAGE	54

Additions to List 54

Air Force Materials Laboratory
Air Force Systems Command
Wright-Patterson Air Force Base, Ohio 45433
Attn: MAAM (Lt. John H. Estess)

Dr. C. H. Church
Westinghouse Electric Corporation
Research Laboratories
Pittsburgh 35, Pennsylvania

Prof. Donald S. McClure
Institute for the Study of Metals
University of Chicago
Chicago 37, Illinois

Dr. Daniel Grafstein
General Precision, Inc.
Aerospace Group
Little Falls, New Jersey

MORE ADDITIONS TO LIST 54

Professor R. C. Ohlmann
Westinghouse Research Laboratories
Pittsburgh, Pennsylvania

Dr. R. C. Linares
Perkin-Elmer Corporation
Solid State Materials Branch
Norwalk, Connecticut 06852

Dr. J. G. Atwood
Perkin-Elmer Corporation
Electro-Optical Division
Norwalk, Connecticut

Professor S. Claesson
Uppsala University
Uppsala, Sweden

FURTHER ADDITIONS TO LIST 54*

Robert L. Parker
National Bureau of Standards
Washington, D.C.

N.D. Schoenberger
Precision Instrument Company
3170 Porter Drive
Palo Alto, California

---

*Authorized by letter

ONR:421:CES:lm
NR 017-708
30 November 1964

ONR:421:FBI:lsp
13 Nov 1964